Rock Mechanics and Rock Engineering (2020) 53:3563–3587
https://doi.org/10.1007/s00603-020-02117-z

ORIGINAL PAPER

Size-dependent Behaviour of Weak Intact Rocks

Hao Zhai[1] · Hossein Masoumi[2] · Mahdi Zoorabadi[3] · Ismet Canbulat[1]

Received: 16 June 2019 / Accepted: 7 April 2020 / Published online: 22 April 2020

Abstract

Characterising the size-dependent behaviour of rock has been a significant challenge in rock engineering particularly during the design of structures on or within a rock mass. Generally, the mechanical characterisation of rock starts at the laboratory scale where the intact rock is tested and then the resulting data is extrapolated to the field conditions using a suitable size effect model. Despite extensive research on the size effect of intact rock, very few have included the weak rocks with low uniaxial compressive strength (UCS). Thus, in this study, the size-dependent behaviour of two different weak rocks namely, Gambier limestone and artificial rock with uniaxial compressive strength of less than 10 MPa were investigated experimentally and analytically. The diameter of the cylindrical Gambier limestone samples varied from 26 to 285 mm while the diameter of artificial rock samples ranged between 26 and 139 mm. For Gambier limestone, the uniaxial compressive, Brazilian and point load experiments were carried out while for artificial rock, only the uniaxial compressive tests were conducted. In both rock types, the ascending and then descending size effect trend was a pronounced behaviour for UCS and Young's modulus data while the size effect behaviour of Poisson's ratio was inconclusive. Also, the tensile strength and point load index data obtained from Gambier limestone revealed only descending size effect trends. The unified size effect law and its improved version were fitted to the UCS and Young's modulus data leading to a very good agreement between the data and the model predictions. It was confirmed that an improved version of unified size effect law can predict a more realistic strength value for a sample with an infinite size. Finally, the applicability of two descending size effect models to the tensile strength and point load data was assessed and concluded that the multifractal scaling law is a suitable model for the point load data while the size effect law can better predict the tensile strength data.

Keywords Weak rock · Size effect · UCS · Young's modulus · PLI · Tensile strength · Ascending then descending trend

List of Symbols

UCS	Uniaxial compressive strength
E	Young's modulus
PLI	Point load index
SD	Standard deviation
CV	Coefficient of variance
USEL	Unified size effect law
IUSEL	Improved version of USEL
SEL	Size effect law
FFSEL	Fractal fracture size effect law
σ_0	Intrinsic strength for the ascending part of USEL
f_t	Characteristic strength for the descending part of USEL
d	Sample size in USEL
d_0	Maximum aggregate size or a characteristic sample size in USEL
B and λ	Dimensionless material parameters in USEL
D_f	Fractal dimension of fracture surface in USEL
MFSL	Multifractal scaling law
MMFSL	Modified multifractal scaling law
l	Material constant with unit of length in IUSEL
f_c	Strength of a sample with an infinite size in IUSEL
f_m	Characteristic strength of the ascending zone in IUSEL
d	Sample size in IUSEL
d_f	Fractal dimension in IUSEL

✉ Hossein Masoumi
hossein.masoumi@monash.edu

[1] School of Minerals and Energy Resources Engineering, UNSW Australia, Sydney, NSW 2052, Australia

[2] Department of Civil Engineering, Monash University, Melbourne, VIC 3800, Australia

[3] Golder Associates, Newcastle, NSW 2304, Australia

K	Correlation factor
k	Constant for Hoek and Brown (1980) size effect model

1 Introduction

The change in size or scale has been proved to have significant effects on the mechanical properties of intact rocks (Hoskins and Horino 1969; Nishimatsu et al. 1969; Symons 1970; Dhir and Sangha 1973; Hoek and Brown 1980; Jackson and Lau 1990; Panek and Fannon 1992; Yuki et al. 1995; Hawkins 1998; Thuro et al. 2001; Pells 2004; Darlington et al. 2011; Masoumi 2013; Masoumi et al. 2016a, b, 2017a, b, 2018; Darbor et al. 2018; Rong et al. 2018; Song et al. 2018; Walton 2018). This is important as often the process of intact rock characterisation starts at the laboratory scale and then extrapolated to the field setting. Considering the limitations associated with the laboratory environment, it is impossible to test an intact rock at the magnitude of field scale within the laboratory. A solution for this limitation is to use an appropriate size effect model which is initially calibrated against the laboratory data and then is used to predict the mechanical properties of intact rock in the range of field scale.

Three main size effect models are currently available in the literature for the extrapolation of laboratory data to the field setting. The first model was introduced by Weibull (1939) based on the statistical theory which the so-called empirical size effect model, proposed by Hoek and Brown (1980) follows this concept. In this theory, the statistical distribution of micro-cracks within a rock with various sizes plays a significant role. The second model was proposed by Bazant (1984) based on fracture energy concept indicating that in a larger sample, the amount of stored energy is higher than that of the smaller one at a same stress level leading to an earlier crack initiation in the larger sample. The third model was developed by Carpinteri () based on fractal theory primarily for the tensile strength of concrete and then the applicability of such a model to rock materials was assessed by Darlington et al. (2011) and Masoumi et al. (2016b, 2017b). The multifractal theory is an extension of self-similarity concept where the size effect can be divided into two physical dimensions, including local and global. The local dimension primarily deals with the very small sizes while the global dimension is associated with an infinite scale. These three models along with the other proposed empirical and semi-empirical functions (Bieniawski 1968; Hoek and Brown 1980; Cunha 1990; Hoek 2000; Darlington et al. 2011) follow the generalised size effect concept in which the strength reduces with an increase in size. Such a concept has been widely investigated and a number of researchers, including Nishimatsu et al. (1969), Hawkins (1998), Masoumi (2013) and Quiñones et al. (2017) revealed that the descending size effect model alone cannot accurately predict the size effect behaviour of intact rocks when a relatively wide range of sample sizes are considered. Hawkins (1998) was the first who clearly demonstrated that the uniaxial compressive strength (UCS) of seven different sedimentary rocks followed an ascending then descending size effect trend, highlighting the limitation of widely used generalised size effect concept. The results from Hawkins (1998) were later endorsed by Masoumi et al. (2016b) who also showed similar strength ascending then descending size effect behaviour for UCS results obtained from Gosford sandstone not only at one slenderness (length to diameter) ratio, but also at other ratios (Masoumi et al. 2014; Roshan et al. 2016).

In order to describe such an ascending then descending size effect behaviour, Unified Size Effect Law (USEL) was initially introduced based on fractal and fracture theories (Bazant 1984, 1997) and later Masoumi et al. (2017b) proposed an improved version of Unified Size Effect Law (IUSEL) based on the only fractal theory. Masoumi et al. (2016b) validated USEL based on the UCS data obtained from Gosford sandstone as well as those reported by Hawkins (1998). Later, Quiñones et al. (2017) demonstrated the applicability of ascending then descending size effect trend to UCS data obtained from some strong igneous rocks with an excellent agreement between the model predictions and the empirical data.

It is noteworthy that the strength ascending then descending behaviour has also been reported by Bahrani and Kaiser (2016) and Li et al. (2018) from numerical studies using discrete element modelling. Faramarzi and Rezaee (2018) performed some uniaxial compressive experiments on a set of cylindrical concrete samples with different sizes and concluded that an ascending then descending strength trend is also applicable to the concrete samples.

From the above review, it is clear that the ascending then descending strength behaviour of intact rocks at different sizes has been extensively investigated in the medium to strong rock types where the UCS of tested rocks was mostly above 10 MPa. Thus, in this study, the size effect behaviour of a number of weak rocks with UCS of less than 10 MPa is investigated at a broad range of diameters from 26 mm to about 285 mm. The rock types were the natural Gambier limestone and artificial rock made of plaster. A set of uniaxial compressive, indirect tensile (or Brazilian) and point load tests was conducted on Gambier limestone while for the artificial rock only the uniaxial compressive experiments were carried out. Also, the reporting data from the literature on the size effect behaviour of a weak rock was included in the final analysis. The resulting UCS data and Young's moduli obtained from Gambier limestone and artificial rock revealed an ascending then descending size effect behaviour which were used to calibrate the USEL and IUSEL for the strength prediction at different sizes. In addition, it was demonstrated that IUSEL provides more realistic UCS and Young's modulus prediction for a rock sample with an infinite scale. On the other hand, the point load and tensile strength results obtained from Gambier limestone showed only a descending size effect behaviour which then the applicability of SEL and MFSL to the point load and tensile strength data was investigated extensively.

2 Experimental Work

2.1 Rock Sample Selection and Preparation

The Gambier limestone, used in this study was sourced from the Mount Gambier coastal region in South Australia. It is a light weight limestone formed in the Paleogene period, 27.5–33 million years ago, from shoreline and marine sediments (Allison and Hughes 1978; Murray-Wallace et al. 1999; Melean et al. 2009). Gambier limestone is a pale light-yellow homogeneous rock with approximately 50% porosity. The X-ray diffraction (XRD) and fluorescence (XRF) were conducted on Gambier limestone (see Fig. 1; Table 1) confirming that it consists of more than 98% calcite. A number of limestone samples were prepared at different diameters (see Fig. 2) ranging between 25 and 285 mm with the length to diameter ratio of 2 for the uniaxial compressive tests according to American Society for Testing and Materials (ASTM 2010). Also, at the same range of diameters some samples were prepared for Brazilian experiments according to ASTM (2010) where the length of samples was half of the diameter (see Fig. 3). For the point load tests, the length to diameter ratio was 1 according to International Society for Rock Mechanics (ISRM 2014).

For the artificial rock samples, a mixture of sand and plaster was used to cast the samples with low strength at various sizes. The final mixture was modified based on the experiments conducted by Dorbani et al. (2011) leading to an artificial rock made of plaster, sand and water at a ratio of 1:2:1.35. An electrical blender and vibrator were used to create a homogenous mixture and remove air pockets from the mixture. The samples were casted using PVC moulds with various diameters (from 26 to 139 mm) and after curing for 24 h (see Fig. 4), they were removed from the moulds

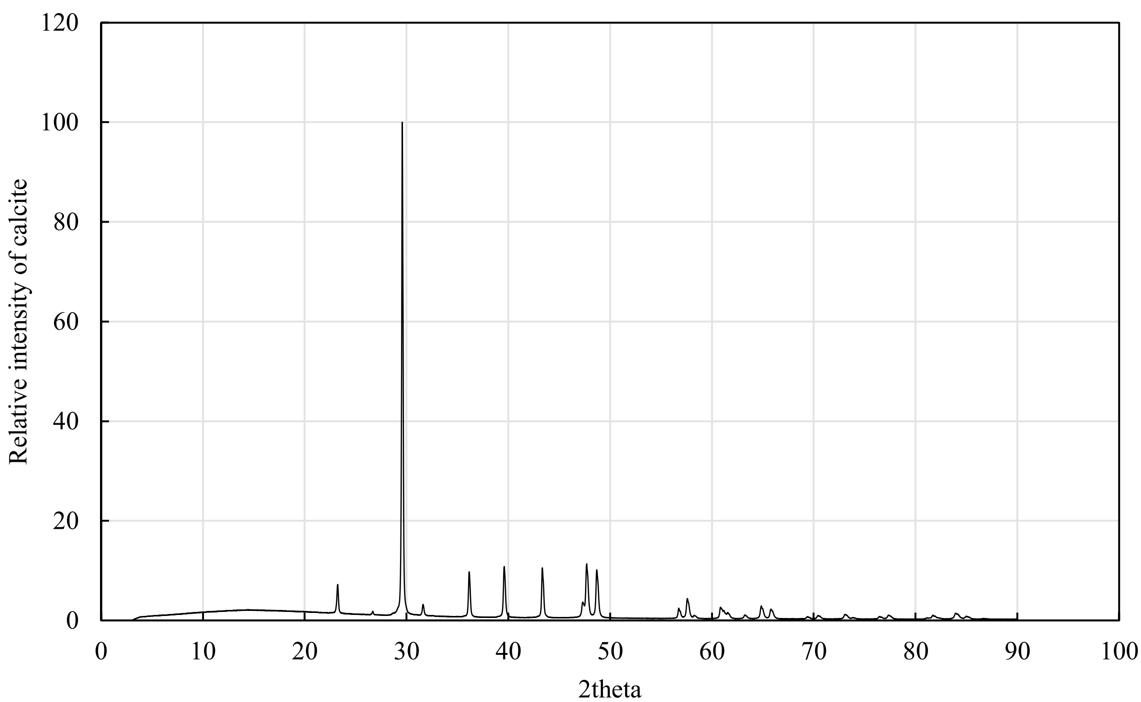

Fig. 1 Diffractometer trace for Gambier limestone

Table 1 X-ray fluorescence results obtained from Gambier limestone

Element	MgO	SiO_2	SO_3	Cl	K_2O	CaO	$Cr2O_3$	$Fe2O_3$	NiO	SrO	ZrO_2	Ba
%	0.64	0.57	0.07	0.01	0.19	98.09	0.10	0.23	0.02	0.05	0.01	0.02

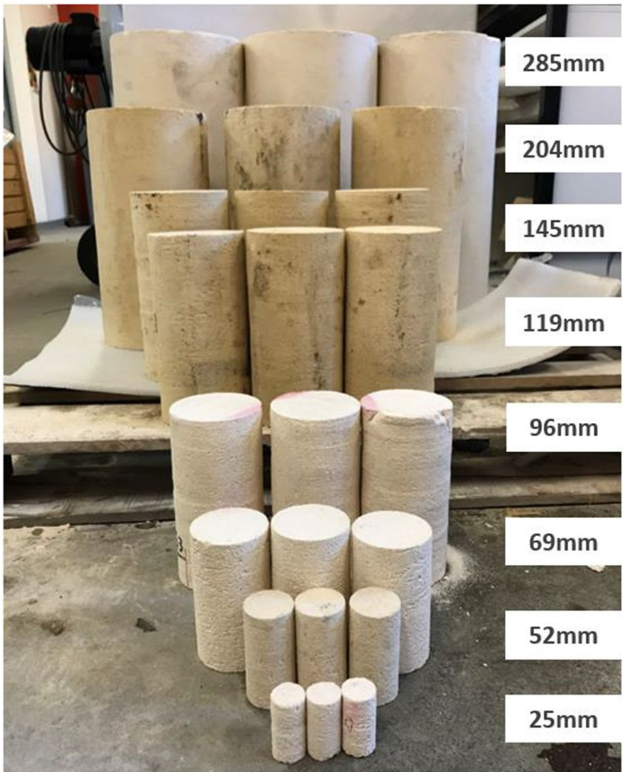

Fig. 2 Examples of Gambier limestone samples with different diameters for uniaxial compressive test

Fig. 3 Examples of Gambier limestone samples with different sizes for Brazilian test

and stored in a well-ventilated and shaded room for 7 days to obtain the required mechanical properties.

In order to reduce the influence of moisture content, all the natural and artificial samples were oven-dried at 105 ℃ and 45℃ respectively for 24 h prior to the experimentation. The drying temperature of artificial samples was less than

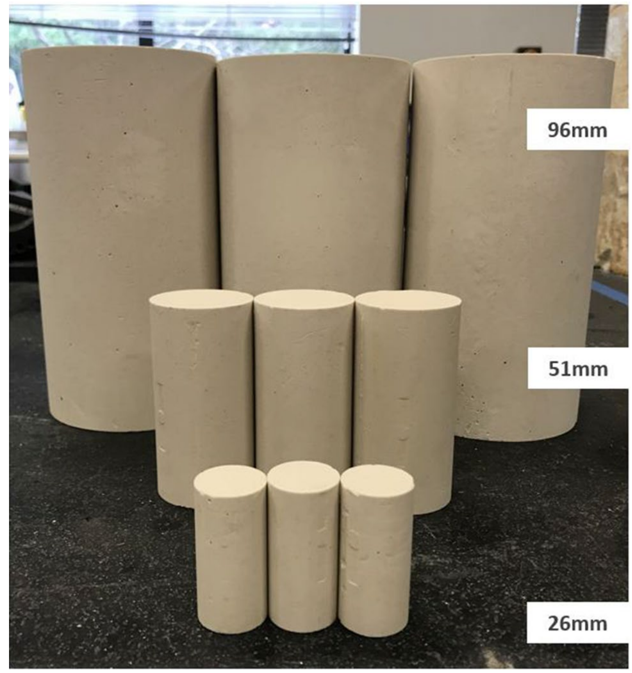

Fig. 4 Examples of artificial rock samples with different diameters for uniaxial compressive test

50 ℃ to ensure the stability of final products according to Ridge (1958) and Clifton (1973).

2.2 Testing Procedure

The uniaxial compressive tests were performed using a servo-controlled loading frame with a maximum loading capacity of 160 tonnes (see Fig. 5). The axial displacement was recorded based on ram movement and only for the samples with less than 150 mm diameter the radial deformation was measured using circumferential linear variable differential transducer (LVDT). This was due to the limitation in the total length of available circumferential LVDT which could not be mounted on the samples larger than 150 mm diameter. The final radial strain was calculated based on Masoumi et al. (2015) suggested modification.

According to ISRM (1978), polished platens were used for the uniaxial compressive experiments. The strain rate was kept constant for all the experiments to allow the failure of samples within 5–10 min as specified by ISRM (1981). By trial and error, the suitable strain rates for limestone and artificial samples were found to be $1 \times 10^{-5}\ s^{-1}$ and $8 \times 10^{-6}\ s^{-1}$, respectively.

The same loading frame which was used for the uniaxial compressive tests was utilised for the Brazilian tests (see Fig. 6) according to ASTM (2010) suggested methods. In order to record the peak loads at high accuracy, a load cell

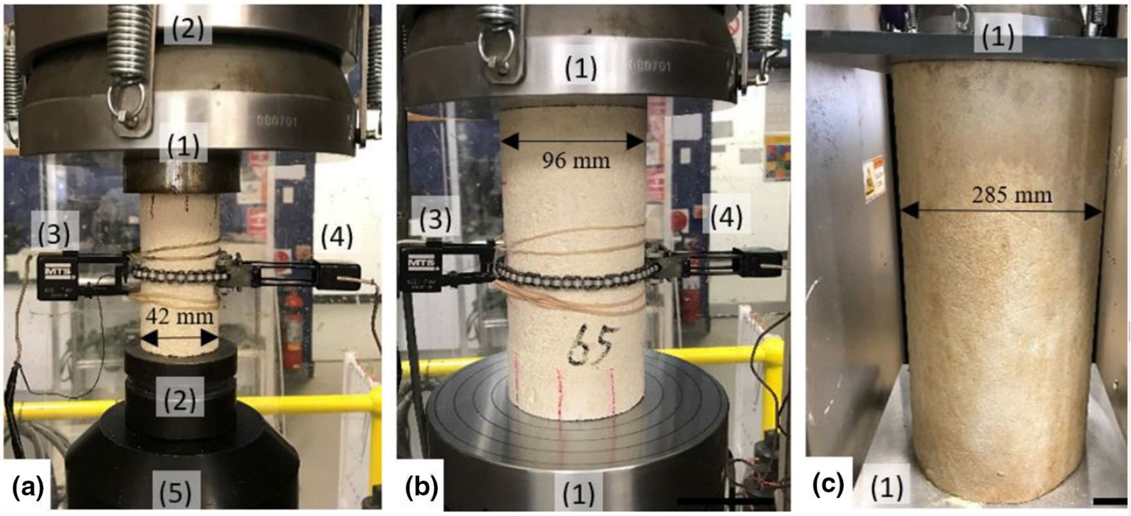

Fig. 5 Testing setup for **a** samples smaller than 70 mm diameter, **b** samples with diameters between 70 and 150 mm and **c** samples larger than 150 mm diameter

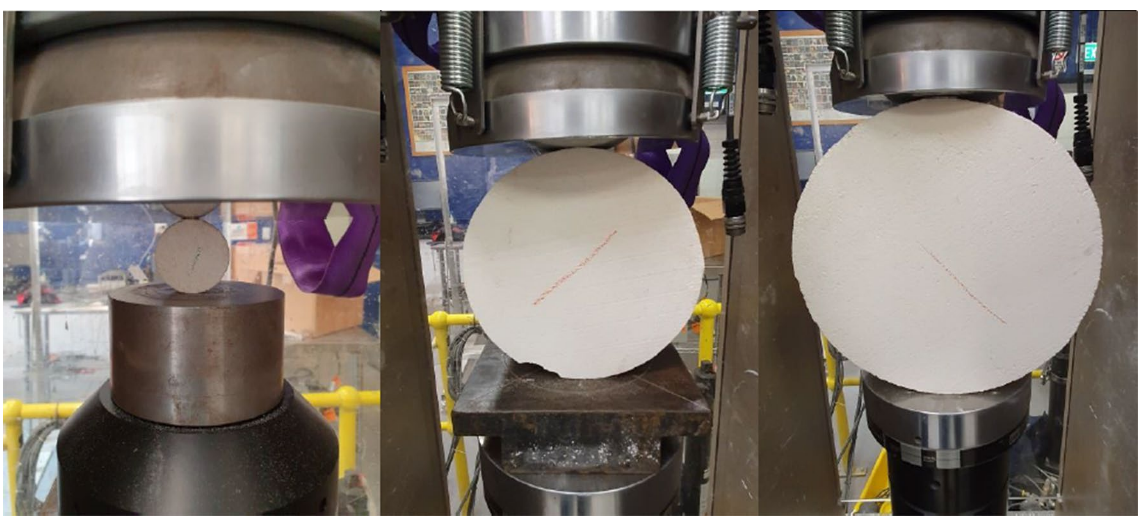

Fig. 6 Examples of different Brazilian testing setups for the samples with various sizes

with the maximum loading capacity of 10 tonne was utilised for the samples smaller than 100 mm diameter.

The point load tests were conducted under two scenarios, including axial and diametral as recommended by ISRM (2014) suggested methods. The GCTS point load frame was used for the experiments and due to the limitation in the loading frame (see Fig. 7), the maximum diameter of tested sample was less than 100 mm.

2.3 Test Results

2.3.1 UCS, Young's Modulus and Poisson's Ratio

The resulting data from uniaxial compressive tests along with the standard deviations (SD) and coefficient of variances (CV) for Gambier limestone and artificial rock samples are given in Tables 2, 3, and 4 including UCS, Young's

Fig. 7 GCTS point load testing frame used for the point load experiments. The arrow indicates the limitation of frame where the sample larger than 100 mm diameter could not be tested

moduli and Poisson's ratios, respectively. Figures 8, 9 and 10 present the size effect trends of UCS, Young's moduli and Poisson's ratios obtained from Gambier limestone in which the UCS and Young moduli clearly revealed an ascending then descending trends while the Poisson's ratio did not follow any particular behaviour. The similar size effect trends as those obtained from Gambier limestone are observable in Figs. 11 and 12 for UCS and Young's moduli of artificial rock, respectively. Figure 13 shows the typical fracture patterns observed after failure of Gambier limestone at various sizes. It is clear that the shear plane is the dominant failure pattern at various sizes and it commonly started from one end surface and then propagated towards the side surface.

From Figs. 8 and 11, it is evident that the UCS of both Gambier limestone and plaster based artificial rock follow an ascending then descending size effect trend in which the UCS increases with an increase in the size up to a characteristic sample diameter, then it reduces beyond this characteristic size. Masoumi et al. (2016b) proposed two mechanisms for such a behaviour. The first one is associated with the end surface flaws which are created during the sample preparation process. This mechanism is the dominant one in the samples with small diameters and granular structure such as sedimentary rocks (Masoumi 2013). The second mechanism is associated with the fractal behaviour of rocks which depends on their geological origins (Masoumi et al. 2016b; Quiñones et al. 2017). A significant difference between the resulting size effect trends from Gambier limestone and artificial rock was at the characteristic size with maximum UCS. Although, both materials are in the same strength range, the characteristic size of Gambier limestone was approximately twice of that obtained from the artificial rock. Based on the earlier studies (Hawkins 1998; Yoshinaka et al. 2008; Pierce et al. 2009; Masoumi et al. 2016b; Quiñones et al. 2017), the difference can be attributed to the intrinsic properties of materials, such as particle size, pre-existing micro-cracks or flaws, texture and more importantly porosity. A comparison between the results from this study and those reported earlier from the medium (Hawkins 1998; Masoumi et al. 2016b) to the strong (Quiñones et al. 2017) rocks confirms that an increase in the UCS can shift the characteristic size to the smaller diameter.

Figures 9 and 12 demonstrate that the size effect trends of Young's moduli for both Gambier limestone and artificial rock have similar behaviour as that observed for UCS data. The similarity was expected as Young's modulus (E) is a function of stress. For both Gambier limestone and artificial

Table 2 UCS and Young's moduli obtained from Gambier limestone at different sizes

Diameter (mm)	Repetition	UCS			Young's modulus		
		Average (MPa)	SD (MPa)	CV (%)	Average (GPa)	SD (GPa)	CV (%)
26	15	2.58	0.57	22.05	0.99	0.49	48.94
41	10	3.02	0.37	12.37	1.01	0.42	41.50
52	10	3.10	0.31	10.13	1.11	0.26	23.13
69	14	3.49	0.39	11.05	1.19	0.14	11.75
96	10	3.72	0.35	9.43	1.26	0.17	13.62
119	4	3.99	0.33	8.38	1.78	0.37	21.01
145	5	3.74	0.17	4.58	1.64	0.31	19.11
204	3	3.14	0.34	10.77	1.65	0.12	7.27
285	3	2.64	0.38	14.44	1.22	0.06	5.27

Table 3 Poisson's ratios obtained from Gambier limestone at different sizes

Diameter (mm)	Repetition	Poisson's ratio		
		Average	SD	CV(%)
26	6	0.13	0.02	14.15
41	5	0.09	0.03	30.48
52	8	0.13	0.01	9.84
69	7	0.09	0.02	26.64
96	7	0.06	0.01	17.63
119	6	0.13	0.03	29.06
145	3	0.07	0.01	18.61

rock, E increased up to a characteristic size then reduced. Also, the characteristic size for both rock types was the same as that reported for UCS. This suggests that the same controlling mechanisms identified for the size effect trend of UCS can be responsible for the size-dependent behaviour of Young's modulus. Masoumi (2013) and Quiñones et al. (2017) reported ascending then descending size effect trends for the Young's modulus of different medium to strong rock types such as sandstone, granite and marble.

Figure 10 shows that the size effect trend of Poisson's ratio is inconclusive as it is not possible to extract any particular correlation between the Poisson's ratio and the size. This is consistent with the findings of earlier studies (Masoumi 2013; Quiñones et al. 2017) who reported an inconclusive trend for the size effect behaviour of Poisson's ratio obtained from different medium to strong rock types.

Table 4 UCS and Young's moduli obtained from artificial rock at different sizes

Diameter (mm)	Repetition	UCS			Young's modulus		
		Average (MPa)	SD (MPa)	CV (%)	Average (GPa)	SD (GPa)	CV (%)
26	5	3.09	0.48	15.47	0.92	0.12	13.07
41	5	3.58	0.26	7.36	1.24	0.18	14.54
51	5	3.94	0.16	4.07	1.80	0.18	10.23
68	5	3.26	0.3	9.33	1.61	0.17	10.62
96	3	3.08	0.32	10.36	1.55	0.11	6.94
118	3	2.68	0.02	0.66	1.41	0.09	6.21
139	3	2.52	0.21	8.29	1.17	0.05	4.56

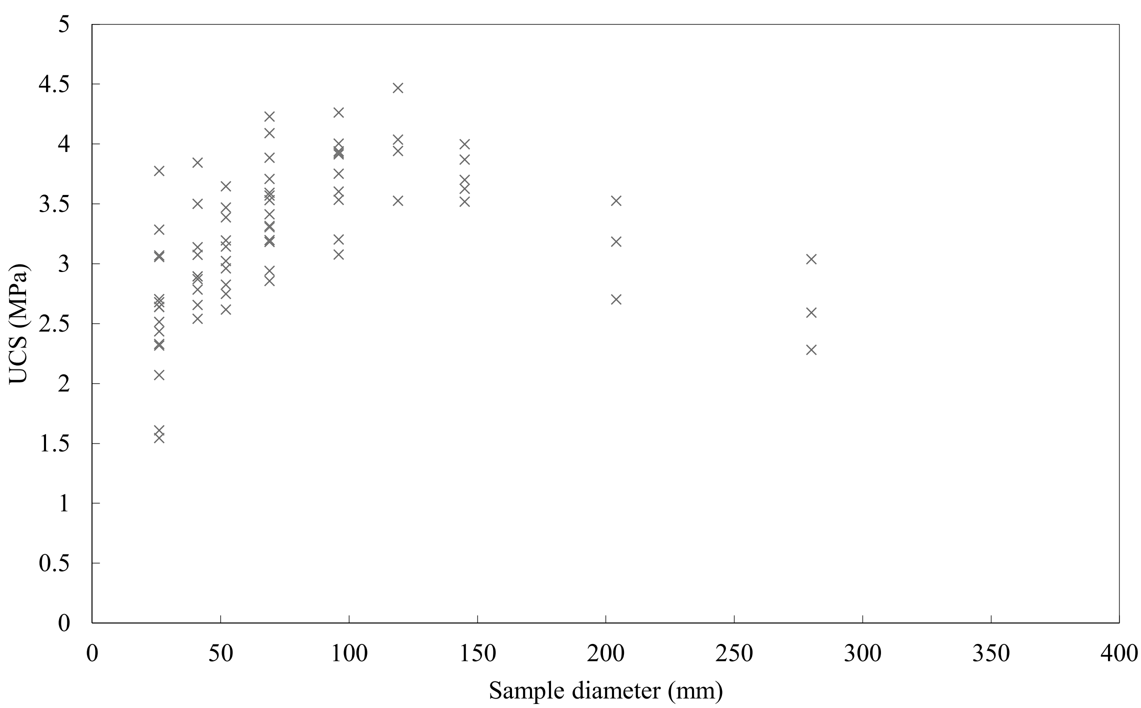

Fig. 8 UCS data obtained from Gambier limestone at various diameters

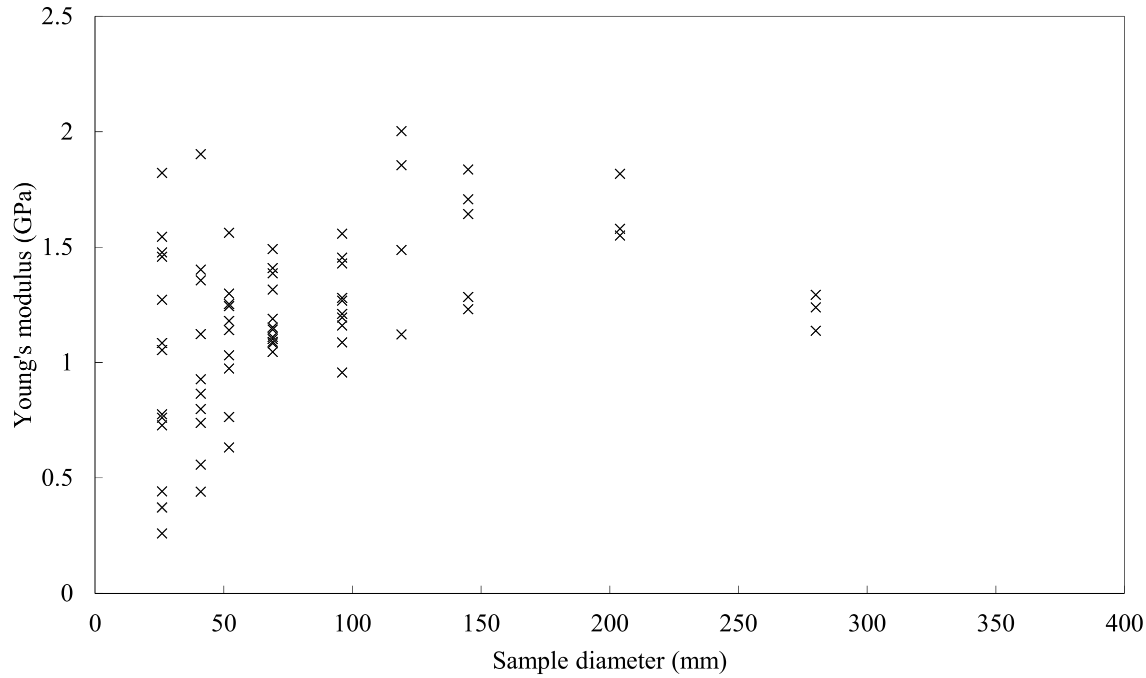

Fig. 9 Young's moduli obtained from Gambier limestone at various diameters

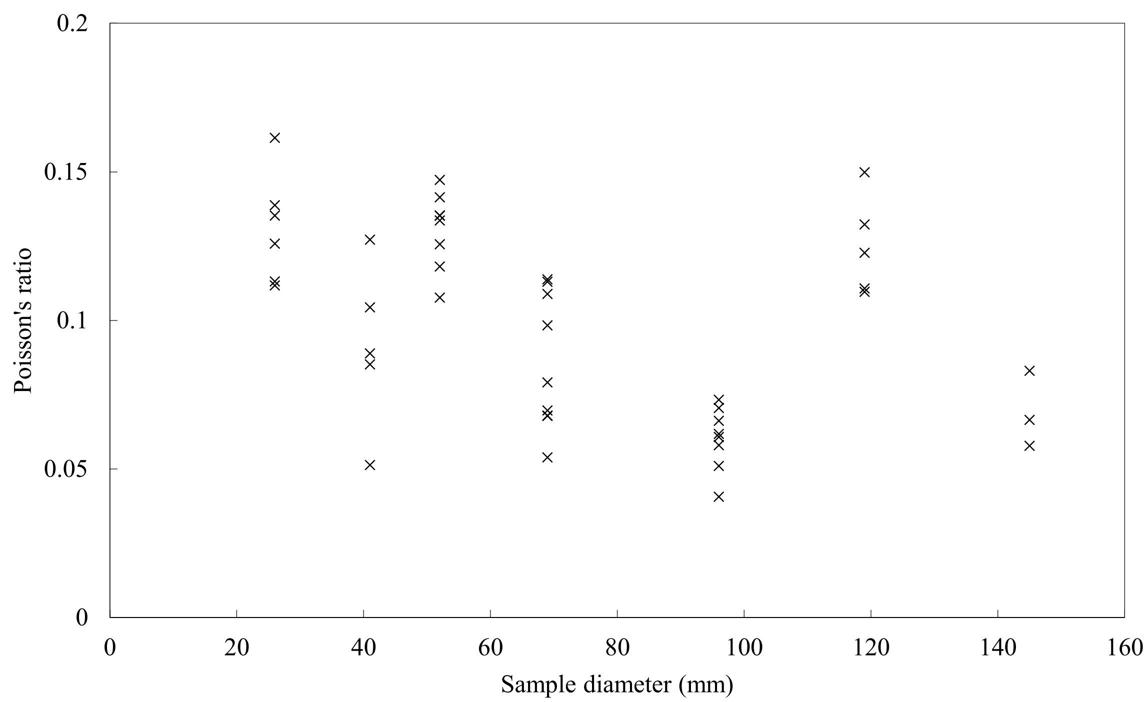

Fig. 10 Poisson's ratios obtained from Gambier limestone at various diameters

2.3.2 Tensile Strength

The resulting tensile strengths at different sizes along with their SDs and CVs for Gambier limestone are presented in Table 5. Also, the size effect trend from tensile strength data is shown in Fig. 14 in which the tensile strength reduces with an increase in the sample size following the conventional size effect theory as opposed to UCS and elastic modulus

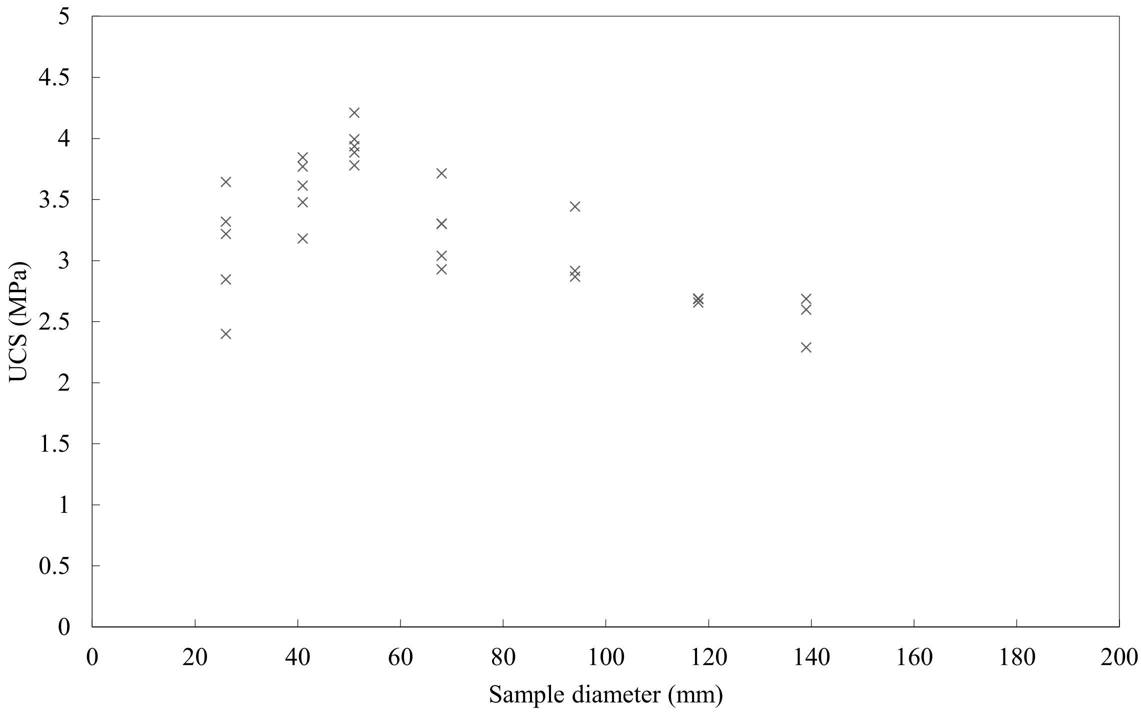

Fig. 11 UCS data obtained from artificial rock at various diameters

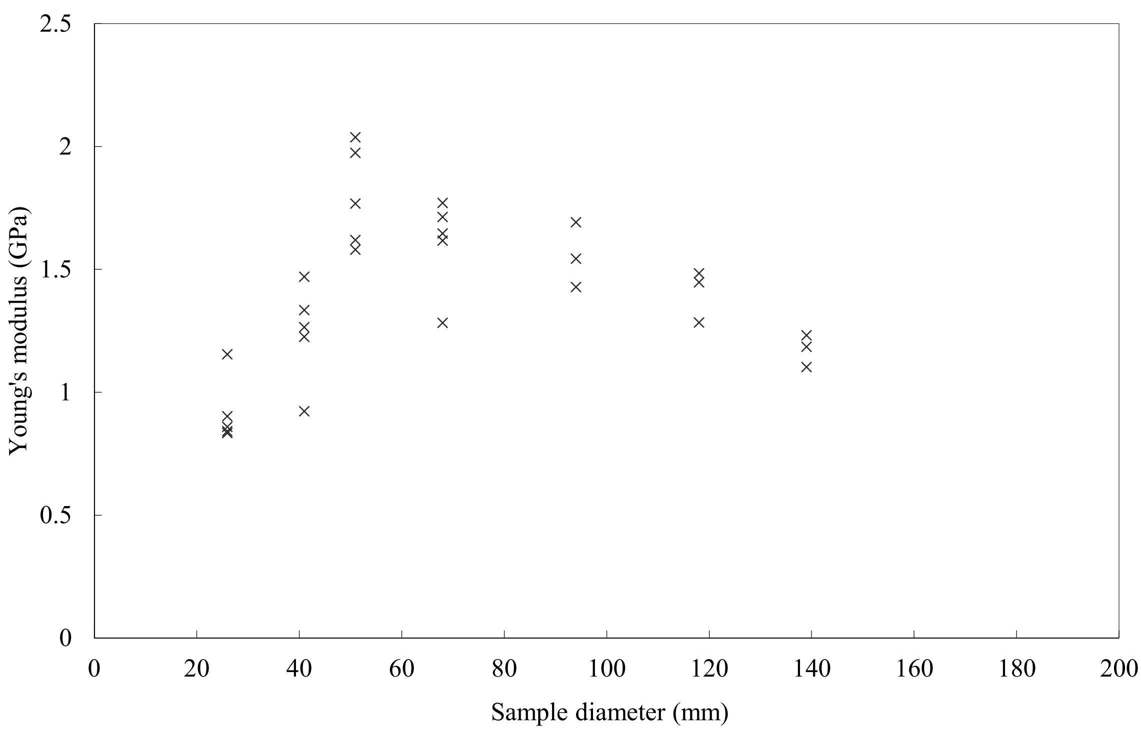

Fig. 12 Young's moduli obtained from artificial rock at various diameters

Fig. 13 Typical failure patterns observed from the uniaxial compressive tests on Gambier limestone with different diameters

data. Such a behaviour can be mainly related to the failure mechanism of rock as well as the contact points between the loading platens and the sample. Masoumi et al. (2016b) argued that the end surface flaws which are created during the cylindrical sample preparation is one of the responsible factors for the strength ascending behaviour of UCS and *E* data. This factor during the Brazilian test cannot be influential as the contact between the sample and the loading platens is different as compared to that in the uniaxial compressive test. In other words, during the Brazilian test, the side surfaces of Brazilian disc are in contact with the loading platens and thus the end surface flaws cannot have any contribution to the failure process. Also, during the Brazilian test, the Gambier limestone sample fails in tension while in the uniaxial compressive loading, the failure occurs primarily in shear (see Fig. 13), therefore, the difference in the failure mechanism between Brazilian and uniaxial compressive tests potentially could be another reason for not observing strength ascending and then descending size effect trend in the tensile strength data. Figure 15 illustrates the typical failure patterns observed from the Brazilian tests on Gambier limestone where all the samples failed in tension with a single crack at the centre.

Table 5 Tensile strength data obtained from Gambier limestone at different sizes

Diameter (mm)	Repetition	Tensile strength		
		Average (MPa)	SD (MPa)	CV (%)
26	6	0.68	0.06	9.40
41	6	0.60	0.09	14.39
52	6	0.62	0.06	10.13
69	6	0.62	0.03	4.32
96	6	0.58	0.06	10.64
119	5	0.55	0.12	20.88
145	5	0.44	0.08	17.76
204	4	0.35	0.03	9.18
285	5	0.34	0.03	8.55

2.3.3 Point Load Index

For the point load experiments, two testing conditions were performed, including axial and diametral. The point load index (PLI) data obtained from both testing conditions are listed in Tables 6 and 7 along with their size effect trends in Figs. 16 and 17, respectively. It is true to state that the behaviour of PLI data at different sizes follows the generalised size effect concept where an increase in the sample size leads to decrease in PLI similar to that observed from the Brazilian tests. Such a behaviour can be associated with the negligible contact between the sample and the pointers during the point loading as well as the failure mechanism of tested samples which is in tension. Russell and Muir Wood (2009) through an extensive analytical and experimental study proved that rock under point loading, primarily fails in tension similar to that observed in the Brazilian test. Also, during the axial point loading, the contact between the end surfaces of sample and the loading platens is very little due to the conical (pointer) shape of platens which can prevent the end surface flaws to contribute to the failure process similar to that explained for the Brazilian test leading to only a descending size effect trend. Figures 18 and 19 illustrate the typical fracture patterns resulted from the point load testing under axial and diametral conditions for Gambier limestone at various sizes.

3 Analytical Work

Masoumi et al. (2016b) proposed the unified size effect law (USEL) to predict the strength ascending then descending behaviour of intact rocks. The USEL consists of two models based on fracture energy and fractal fracture energy. The descending behaviour is predicted by the size effect law (SEL) (Bazant 1984) and the ascending strength behaviour can be predicted by the fractal fracture size effect law (FFSEL) (Bazant 1997). The USEL is the combination of

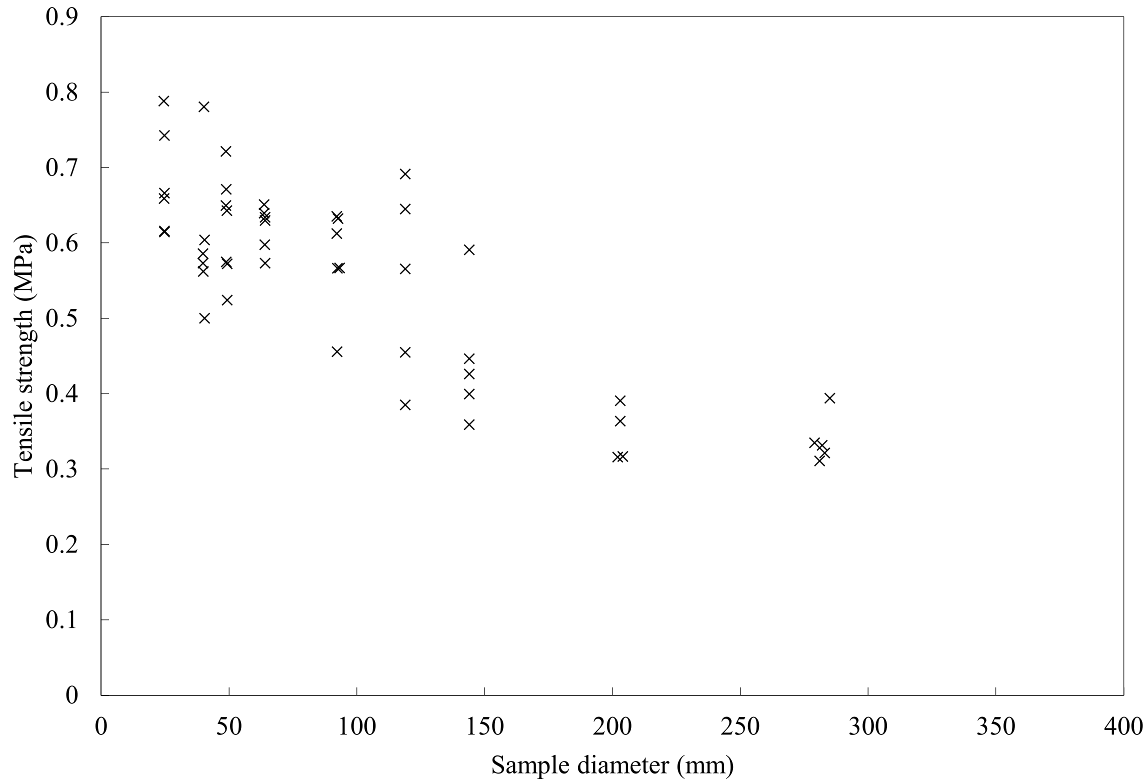

Fig. 14 Tensile strength data obtained from Gambier limestone at various diameters

Fig. 15 Typical failure patterns observed from the Brazilian tests on Gambier limestone

SEL and FFSEL in which the strength, or those parameters which are the function of strength such as Young's modulus, is the minimum estimated value by SEL and FFSEL as follows:

Table 6 Axial PLI data obtained from Gambier limestone at different sizes

Diameter (mm)	Repetition	Axial point load index		
		Average (MPa)	SD (MPa)	CV (%)
26	10	0.76	0.11	14.44
41	5	0.59	0.04	6.37
52	5	0.59	0.04	6.24
69	5	0.56	0.05	8.11
96	5	0.48	0.09	17.72

Table 7 Diametral PLI data obtained from Gambier limestone at different sizes

Diameter (mm)	Repetition	Diametral PLI		
		Average (MPa)	SD (MPa)	CV (%)
26	10	0.88	0.051	5.84
41	5	0.62	0.10	15.65
52	5	0.54	0.05	8.70
69	5	0.43	0.06	14.33
96	5	0.41	0.05	12.68

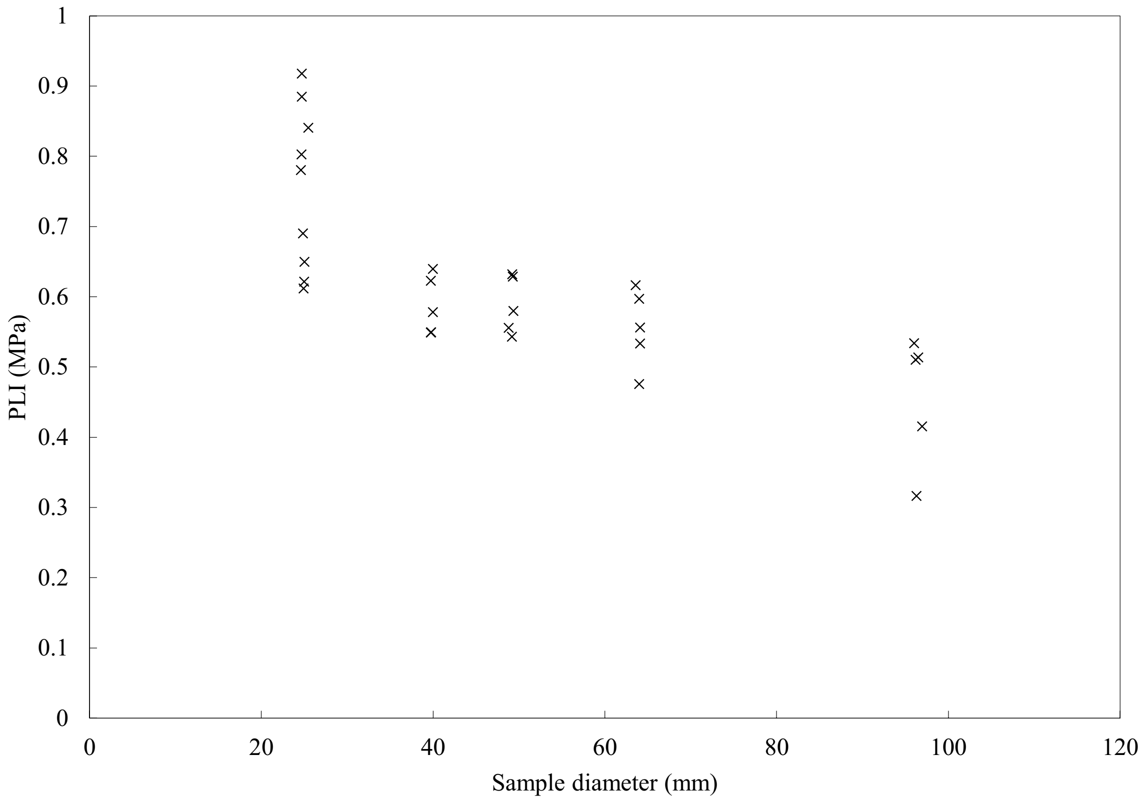

Fig. 16 Axial PLI data obtained from Gambier limestone at various diameters

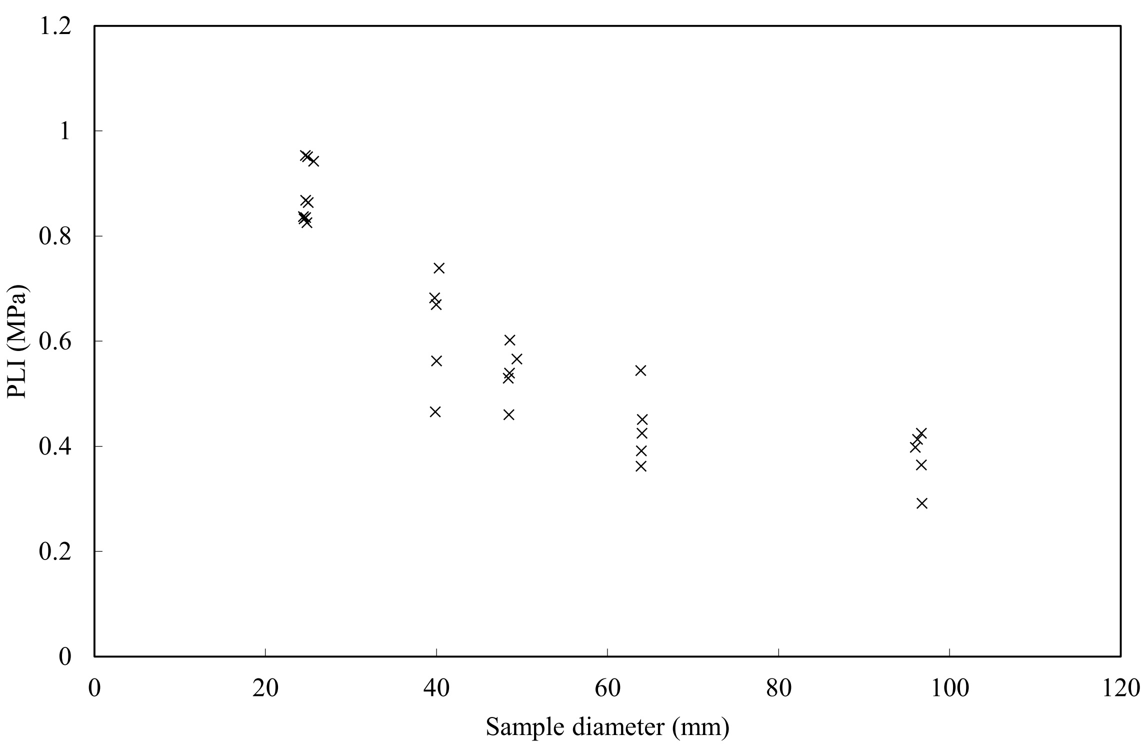

Fig. 17 Diametral PLI data obtained from Gambier limestone at various diameters

Fig. 18 Typical failure patterns observed from the axial point load tests on Gambier limestone

Fig. 19 Typical failure patterns observed from the diametral point load tests on Gambier limestone

$$\text{Strength} = \text{Min}\left(\frac{\sigma_0 d^{(D_f-1)/2}}{\sqrt{1+(d/\lambda d_0)}}(\text{FFSEL}),\ \frac{Bf_t}{\sqrt{1+(d/\lambda d_0)}}(\text{SEL})\right), \quad (1)$$

where σ_0 is the characteristic or intrinsic strength for the ascending zone, f_t is an intrinsic or characteristic strength for the descending zone, d is the sample size, d_0 is a maximum aggregate size which can be referred to as a characteristic sample size, B and λ are the dimensionless material parameters and D_f is the fractal dimension of the fracture surface where $D_f \neq 1$ for the fractal surfaces and $D_f = 1$ for the non-fractal surfaces. For calibration of σ_0 and D_f in FFSEL, initially λd_0 should be attained from SEL. It is noteworthy that FFSEL becomes the same as SEL for those sizes that exhibit non-fractal characteristics ($D_f = 1$), in which $Bf_t = \sigma_0$. Also, the intersection between SEL and FFSEL happens at the following diameter:

$$D_i = \left(\frac{Bf_t}{\sigma_0}\right)^{2/(D_f-1)}, \quad (2)$$

and the maximum strength at D_i is estimated through the following equation:

$$\text{Strength} = \frac{Bf_t}{\sqrt{1+\left((Bf_t/\sigma_0)^{2/(D_f-1)}/\lambda d_0\right)}}. \quad (3)$$

Later, Masoumi et al. (2017b) proposed an improved version of USEL (IUSEL) based on fractal theory consisting of two models to capture the strength ascending and then descending zones, separately. The descending model was developed by Carpinteri et al. (1999), known as the multifractal scaling law (MFSL) and the ascending model was developed by Masoumi et al. (2017b), known as modified multifractal scaling law (MMFSL), in the same fashion as that conducted by Bazant (1997) leading to the following formulae:

$$\text{Strength} = \text{Min}\left(f_m d^{(d_f-1)/2}\sqrt{1+\frac{l}{d}}(\text{MMFSL}),\ f_c\sqrt{1+\frac{l}{d}}(\text{MFSL})\right), \quad (4)$$

where l is a material constant with the unit of length, f_c is the strength of a sample with an infinite size, f_m is a characteristic strength of the ascending zone, d is the sample size and d_f is a fractal dimension. Similar to USEL, it is necessary to estimate l from MFSL first then calibrate f_m and d_f. The maximum strength at the intersection diameter of MFSL and MMFSL occurs when:

$$d_i = \left(\frac{f_c}{f_m}\right)^{2/(d_f-1)}, \quad (5)$$

and the strength is predicted according to:

$$\text{Strength} = f_c\sqrt{1+\frac{l}{\left(\frac{f_c}{f_m}\right)^{2/(d_f-1)}}}. \quad (6)$$

A significant advantage of IUSEL over USEL is a realistic prediction of sample strength with an infinite size. In USEL, the strength of a very large diameter sample tends to zero while IUSEL predicts a constant value (f_c) for a sample with an infinite size. Here, the data from Gambier limestone, artificial rock and Bath stone with a UCS of about 15 MPa

Table 8 Calibrated USEL and IUSEL parameters for UCS results obtained from Gambier limestone

Fitting method	Bf_t (MPa)	λd_0 (mm)	σ_0 (MPa)	D_f	Diameter of sample with the maximum UCS (mm)	Diameter at the intersection (mm)
USEL						
Maximum UCS included in FFSEL	38.06	1.40	0.95	2.53	119	124.48
Maximum UCS included in SEL	13.93	10.87	0.50	2.38		124.22
Maximum UCS included in both	13.93	10.87	0.48	2.40		122.91
Fitting method	f_c (MPa)	l (mm)	f_m (MPa)	d_f	Diameter of sample with the maximum UCS (mm)	Diameter at intersection (mm)
IUSEL						
Maximum UCS included in MMFSL	0.28	25,278.80	N/A	N/A	119	N/A
Maximum UCS included in MFSL	0.68	4041.65	0.016	2.54		130.25
Maximum UCS included in both	0.68	4041.65	0.017	2.54		120.39

Table 9 Calibrated USEL and IUSEL parameters for UCS results obtained from artificial rock

Fitting method	Bf_t (MPa)	λd_0 (mm)	σ_0 (MPa)	D_f	Diameter of sample with the maximum UCS (mm)	Diameter at the intersection (mm)
USEL						
Maximum UCS included in FFSEL	5.54	37.85	0.56	2.21	51	44.17
Maximum UCS included in both	8.52	13.19	0.5	2.45		49.95
Fitting method	f_c (MPa)	l (mm)	f_m (MPa)	d_f	Diameter of sample with the maximum UCS (mm)	Diameter at the intersection (mm)
IUSEL						
Maximum UCS included in MMFSL	1.52	256.26	0.070	2.59	51	48.02
Maximum UCS included in both	1.21	472.59	0.048	2.64		51.19

Table 10 Calibrated USEL and IUSEL parameters for UCS results obtained from Bath stone (Hawkins 1998)

Fitting method	Bf_t (MPa)	λd_0 (mm)	σ_0 (MPa)	D_f	Diameter of sample with the maximum UCS (mm)	Diameter at the intersection (mm)
USEL						
Maximum UCS included in FFSEL	71.38	3.77	3.61	2.35	54	83.20
Maximum UCS included in SEL	19.18	93.64	1.71	2.28		43.69
Maximum UCS included in both	71.38	3.77	1.51	2.91		56.70
Fitting method	f_c (MPa)	l (mm)	f_m (MPa)	d_f	Diameter of sample with the maximum UCS (mm)	Diameter at the intersection (mm)
IUSEL						
Maximum UCS included in MMFSL	9.02	114.59	0.26	2.83	54	48.22
Maximum UCS included in MFSL	4.61	775.96	0.19	2.47		76.61
Maximum UCS included in both	4.61	775.96	0.08	3		57.63

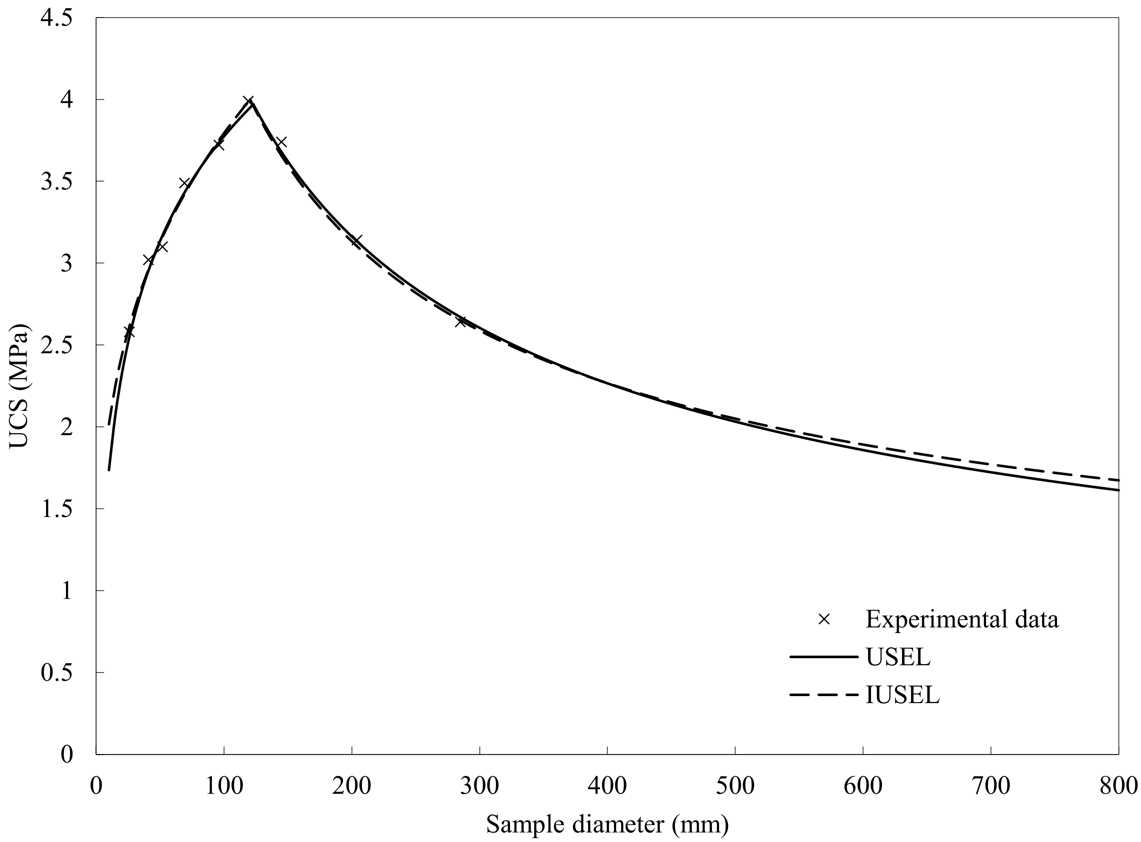

Fig. 20 USEL and IUSEL predictions for UCS data obtained from Gambier limestone

reported by Hawkins (1998) was used to calibrate USEL and IUSEL for the assessment of their predictability.

3.1 Model Predictions for UCS Data

A key concern in the calibration of USEL and IUSEL is the inclusion of characteristic size or the maximum UCS in the modelling process which can occur under three scenarios. First, it is only included in the ascending zone (e.g. FFSEL or MMFSL), second it is only included in the descending zone (e.g. SEL or MFSL) and third it is included in both ascending and descending zones. All the three scenarios were assessed for the modelling process leading to the model parameters listed in Tables 8, 9 and 10 for Gambier limestone, artificial rock and Bath stone, respectively. It is noteworthy that due to the limited data available in the ascending zone of artificial rock, the second scenario could not be assessed. Also, the reported mean UCS values in Tables 2 and 4 were used for the models calibration. For all the three rock types, the best estimation of the intersection diameter occurred when the maximum UCS (characteristic size) was included in both ascending and descending zones. These scenarios are highlighted in bold in Tables 8, 9 and 10 which then they were used for the model simulations as shown in Figs. 20, 21 and 22.

Figures 20, 21 and 22 demonstrate a good agreement between the model predictions and the experimental data for both USEL and IUSEL. Also, it is clear that IUSEL at larger scales starts to deviate from USEL leading to more accurate UCS prediction for the sample with an infinite size. Such a deviation is particularly obvious in Figs. 21 and 22.

As a result, it is reasonable to conclude that the strength ascending then descending trend is applicable to all rock materials when a relatively wide range of sizes are used in the size effect study. This finding is very important for the design process of various structures within the rock masses when the laboratory data is extrapolated to the field conditions. It is important to note that both ISRM (1981) and ASTM (2010) recommend the application of a sample with a diameter of 50–54 mm for uniaxial compressive testing. While such a diameter is reasonable for artificial rock and

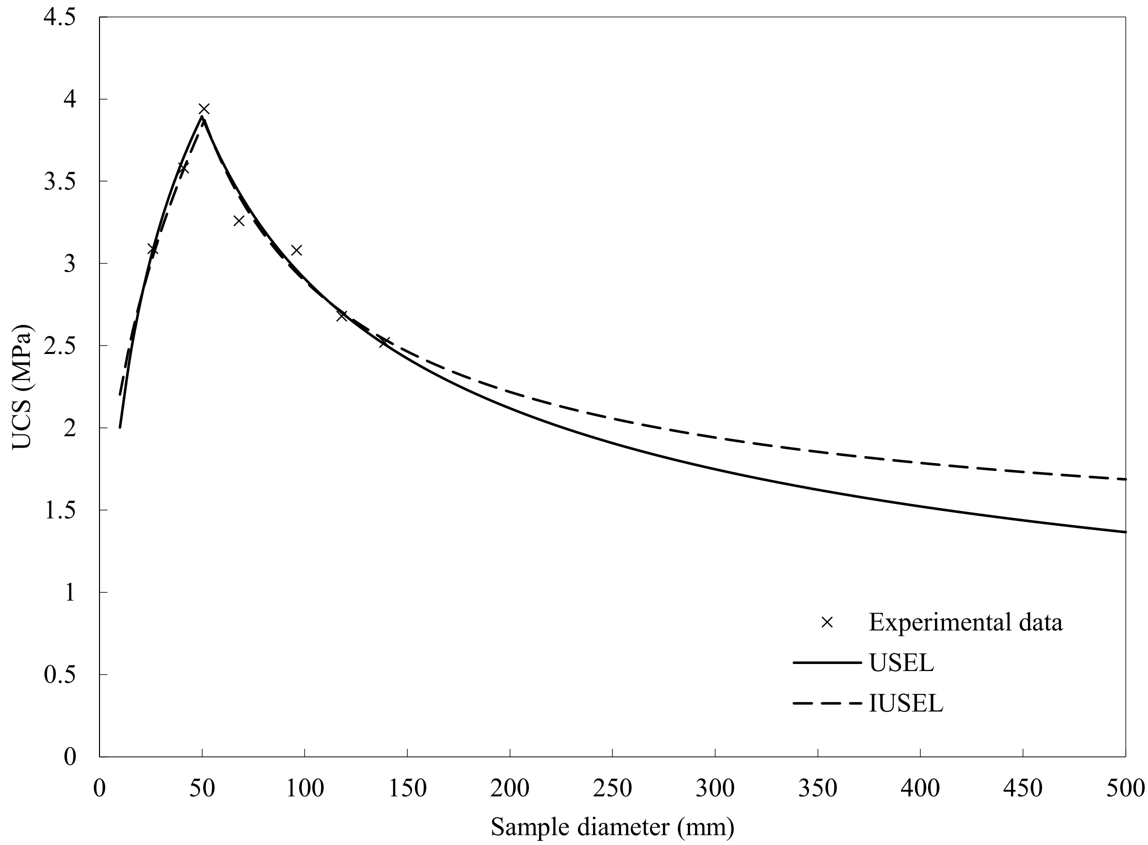

Fig. 21 USEL and IUSEL predictions for UCS data obtained from artificial rock

Bath stone (see Figs. 21, 22), it can potentially lead to an underestimation of UCS of large-scale Gambier limestone and those rock types where the maximum UCS occurs at a sample larger than 50 mm diameter if only the conventional descending size effect model is used for the size correction.

3.2 Model Predictions for Young's Moduli

The applicability of USEL and IUSEL is assessed for Young's modulus following the same method used for the UCS data above. The USEL and IUSEL were calibrated to the Young's moduli of the Gambier limestone and artificial rock leading to the size effect predictive models (see Figs. 23, 24). The resulting models' parameters after calibration are listed in Tables 11 and 12 for Gambier limestone and artificial rock, respectively. Among the three scenarios for including the characteristic size (the size with the maximum Young's modulus), the one where it included in both ascending and descending zones was found to be the best option for both rock types with an exception of IUSEL for artificial rock.

Figures 23 and 24 reveal a good agreement between the fitted models and the experimental results for both USEL and IUSEL. Similar to UCS data, IUSEL provides a more realistic Elastic modulus prediction as compared to USEL for the sample with an infinite size.

3.3 Model Predictions for Tensile Strength and PLI Data

The resulting data from Brazilian and point load testing revealed only descending size effect trend and thus SEL and MFSL have been calibrated against the experimental results to compare their predictability for each set of data. It is noteworthy that Hoek and Brown (1980) size effect model was not included in this analysis due to its simple equation where only one factor controls the modelling process while for SEL and MFSL there are two different factors.

The resulting parameters for SEL and MFSL after model calibration versus tensile strength and PLI data are presented in Table 13 along with their multiple determination

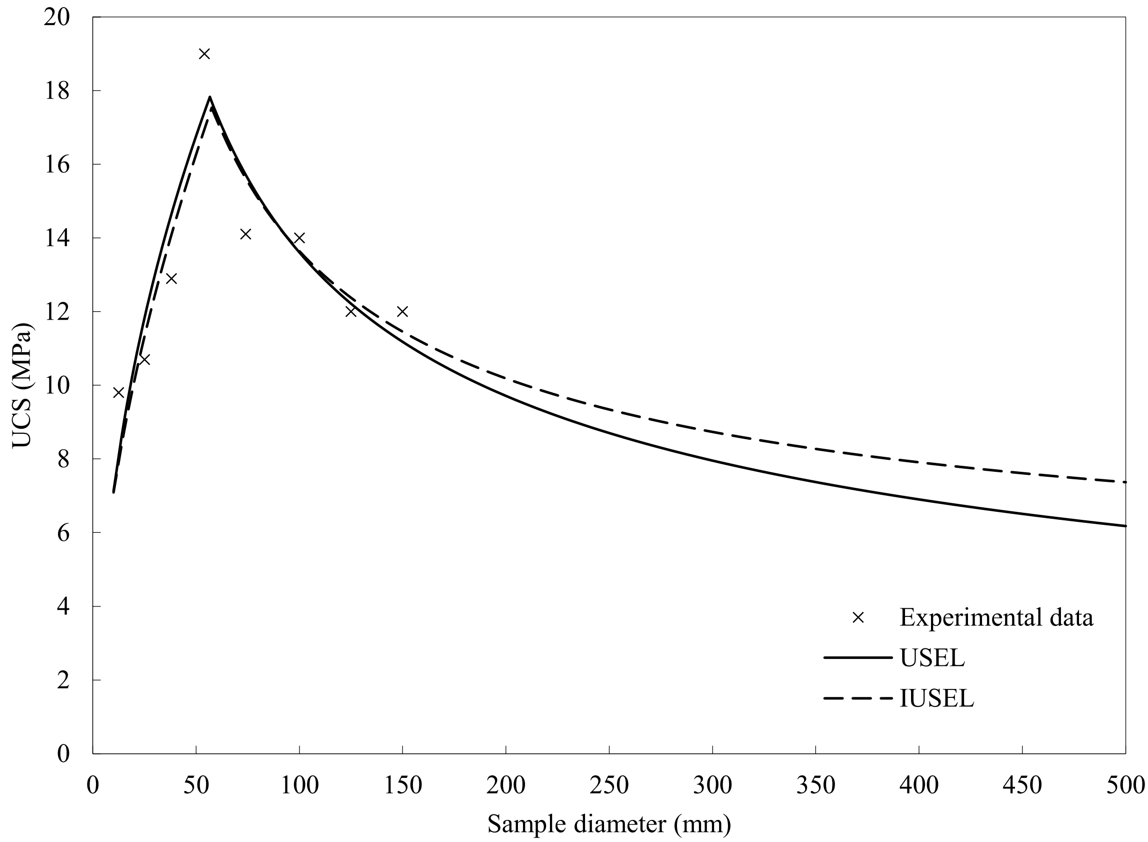

Fig. 22 USEL and IUSEL predictions for UCS data obtained from bath stone (Hawkins 1998)

coefficients (R^2). Also, the fitted models are presented in Figs. 25 and 26 where there is a very good agreement between the fitted models and the laboratory data. It is true to state that SEL has a better predictability to tensile strength data while MFSL found to be a better size effect model for both axial and diametral PLI data obtained from Gambier limestone.

4 Practical Study

The last and very important analysis in this work is to highlight the practical application of size effect correction associated with the weak intact rock. Tunnelling is one of the most critical areas in rock engineering that the results from this study provides a very useful guideline for the rock engineers particularly during the design stage. Road construction in weak rock is another area where the size effect behaviour of weak intact rock becomes important in which the blasting and stability of weak rock slope are the key concerns. Successful construction and stability assessment of hydro-tunnels as well as shallow open-pit (e.g. coal or quarry) mines are other examples that depend on the accurate size correction analysis in weak rocks. Therefore, in the following sections, a useful practical methodology for the correlation between PLI and UCS at different sizes along with an example of miscalculation of size effect due to the utilisation of poor size effect model are presented.

4.1 Correlation Between UCS and PLI Data

In many rock engineering projects, the assessment of intact rock starts with a simple field-testing technique, such as point loading. According to ISRM (2014) suggested methods, UCS and PLI can be correlated using the following equation:

$$\mathrm{UCS} = K \cdot \mathrm{PLI}, \tag{7}$$

where K is a correlation factor suggested by ISRM (2014). Thus, in here the resulting PLI data were correlated with the UCS data obtained from Gambier limestone at various

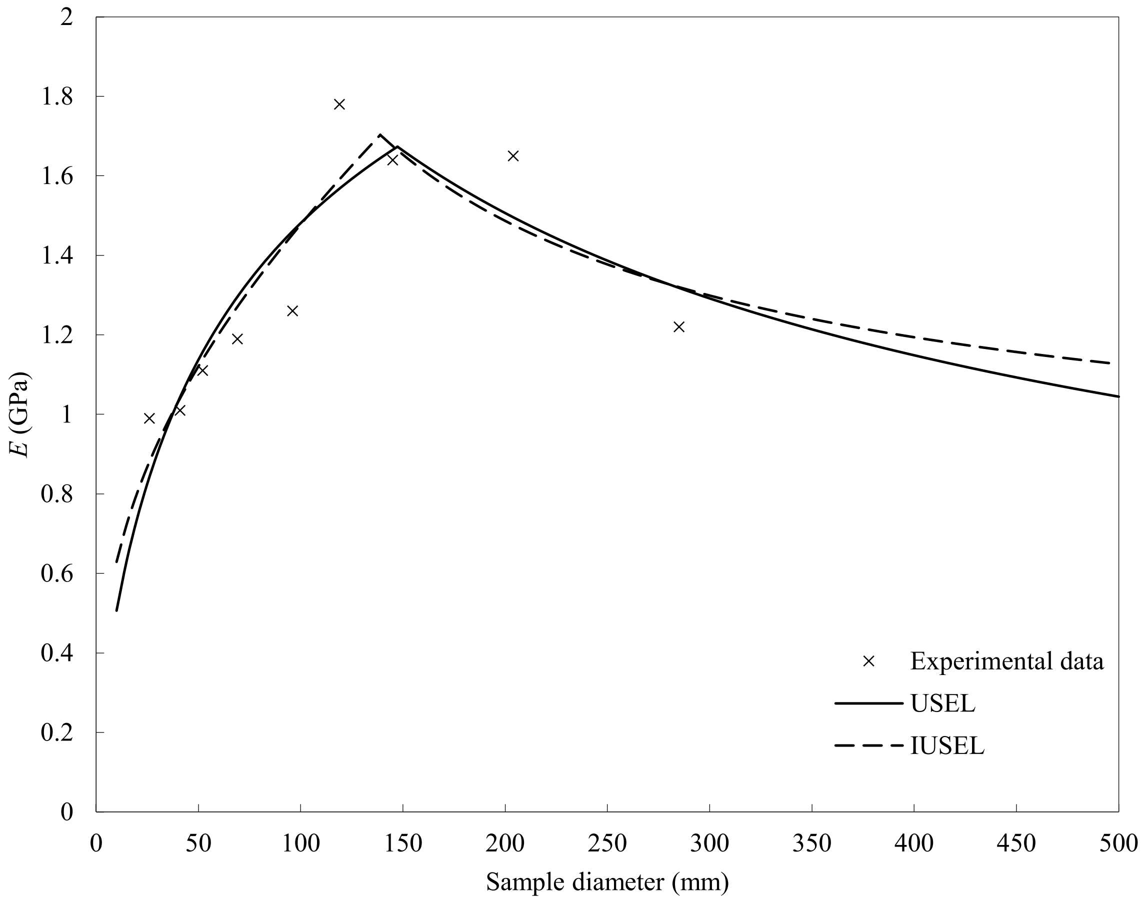

Fig. 23 USEL and IUSEL predictions for Young's moduli obtained from Gambier limestone

sizes (see Table 14). The correlations include both axial and diametral point load data where for each size and loading condition, K is different (Fig. 27).

In another analysis, the graphs of correlation factor versus sample diameter for both axial and diametral conditions were plotted along with their best linear fits in Figs. 28 and 29. It is clear that a linear correlation can provide a good estimation between size and K which can assist in estimation of UCS from point load results (either axial or diametral) with suitable size correction process. This has been conducted on Gambier limestone as a base technique to be used for other weak intact rocks with the similar characteristics as Gambier limestone.

4.2 Example of Application

In this section, a simple practical example for estimating the UCS of Gambier limestone samples with different sizes is demonstrated using the Hoek and Brown (1980) size effect model and the results are compared with the data from this investigation.

The mean UCS of Gambier limestone samples with 52 mm diameter reported in Table 2 ($UCS_{52} = 3.10$ MPa) was substituted into the Hoek and Brown (1980) size effect model as the characteristic strength of a sample with 50 mm diameter (UCS_{50}) in order to estimate the UCS of other sizes using the following equation:

$$UCS = UCS_{50}(50/d)^k. \quad (8)$$

where k is a constant and according to Hoek and Brown (1980) who collated the size effect data from various rock types (where no weak rock was included), this value is equal to 0.18 for all rock types. The fitted Hoek and Brown (1980) size effect model to Gambier limestone data is shown in Fig. 30 indicating that Hoek and Brown (1980) size effect model grossly over-predicts the UCS below 50 mm diameter and under-predict the UCS above 50 mm diameter. This under-prediction would be significant if the data is

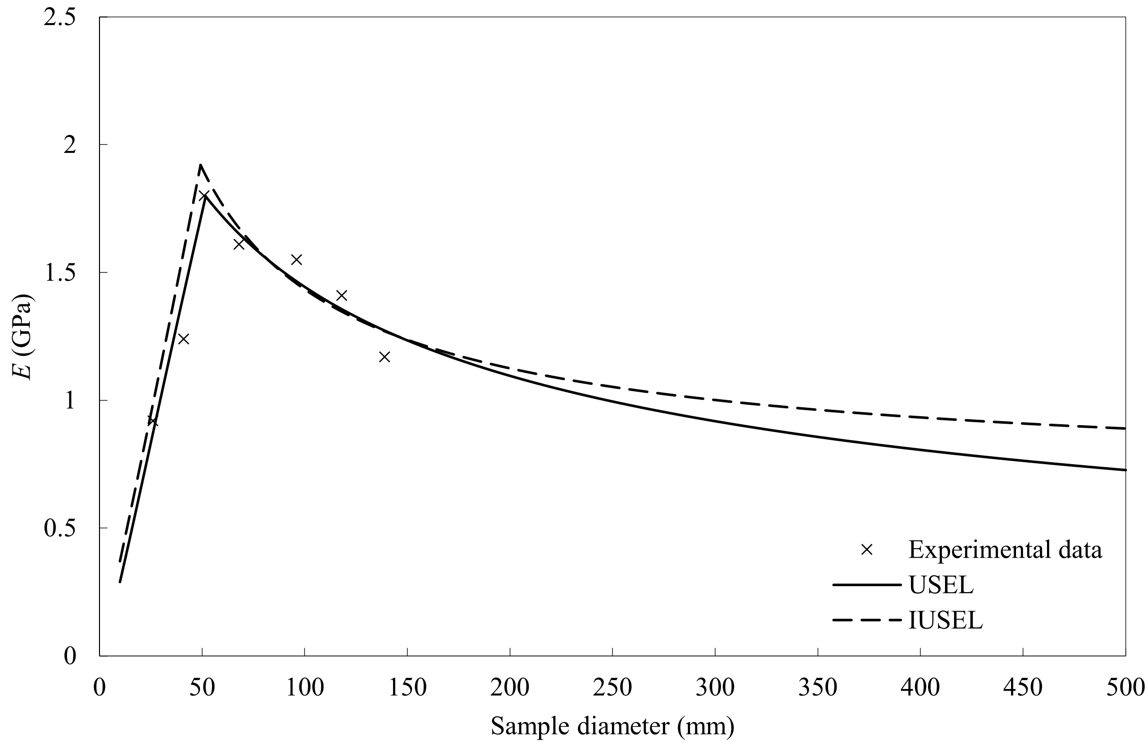

Fig. 24 USEL and IUSEL predictions for Young's moduli obtained from artificial rock

Table 11 Calibrated USEL and IUSEL parameters for Young's moduli obtained from Gambier limestone

Fitting method	Bf_t (GPa)	λd_0 (mm)	σ_0 (GPa)	D_f	Diameter of sample with the maximum E (mm)	Diameter at the intersection (mm)
USEL						
Maximum E included in FFSEL	3.09	62.99	0.122	2.29	119	150.01
Maximum E included in SEL	2.85	77.52	0.290	1.81		282.15
Maximum E included in both	2.85	77.52	0.129	2.24		147.28
Fitting method	f_c (GPa)	l (mm)	f_m (GPa)	d_f	Diameter of sample with the maximum E (mm)	Diameter at the intersection (mm)
IUSEL						
Maximum E included in MMFSL	0.64	906.10	0.009	2.72	119	142.37
Maximum E included in MFSL	0.80	490.37	0.026	2.31		187.04
Maximum E included in both	0.80	490.37	0.013	2.67		138.90

extrapolated to a much larger block size as is done with the Hoek and Brown (1980) size effect relationship in practice. This could lead to overdesign of structures in or on rock and thus it is important to test the large cores from the site investigation.

5 Conclusions

Size-dependent behaviour of two weak intact rocks including Gambier limestone and artificial rock was investigated from experimental and analytical viewpoints. The sample sizes varied from 26 to 285 mm diameter for Gambier

Table 12 Calibrated USEL and IUSEL parameters for Young's moduli obtained from artificial rock

	Bf_t (GPa)	λd_0 (mm)	σ_0 (GPa)	D_f	Diameter of sample with the maximum *E* (mm)	Diameter at the intersection (mm)
USEL						
Maximum *E* included in FFSEL	2.88	33.45	0.015	3.63	51	54.50
Maximum *E* included in both	2.81	35.84	0.016	3.62		51.69
	f_c (GPa)	l (mm)	f_m (GPa)	d_f	Diameter of sample with the maximum *E* (mm)	Diameter at the intersection (mm)
IUSEL						
Maximum *E* included in MMFSL	0.69	331.68	0.002	4	51	49.19
Maximum *E* included in both	0.82	203.83	0.002	3.95		59.07

Table 13 SEL and MFSL parameters for tensile strength and PLI data obtained from Gambier limestone

	SEL			MFSL		
	Bf_t (MPa)	λd_0 (mm)	R^2	f_c (MPa)	l (mm)	R^2
Tensile strength	0.81	72.14	0.88	0.36	83.56	0.69
Axial PLI	1.08	22.74	0.90	0.35	92.04	0.94
Diametral PLI	19.18	0.05	0.92	0.02	35,271.89	0.93

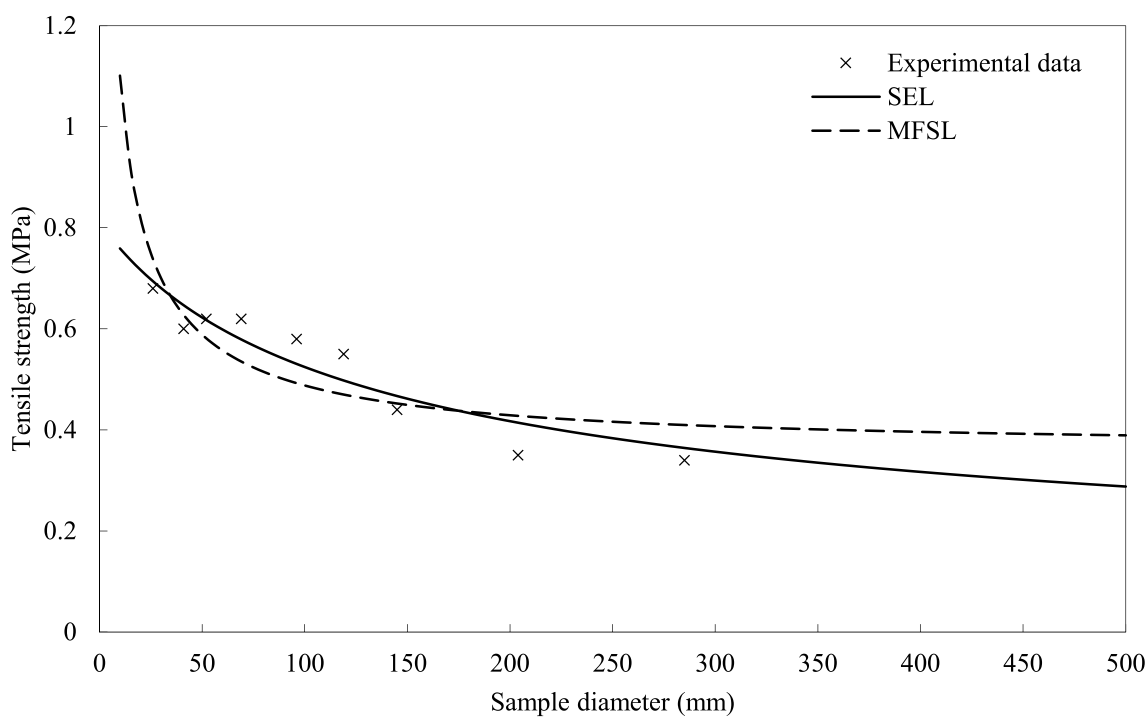

Fig. 25 Comparing SEL and MFSL predictions for tensile strength data obtained from Gambier limestone

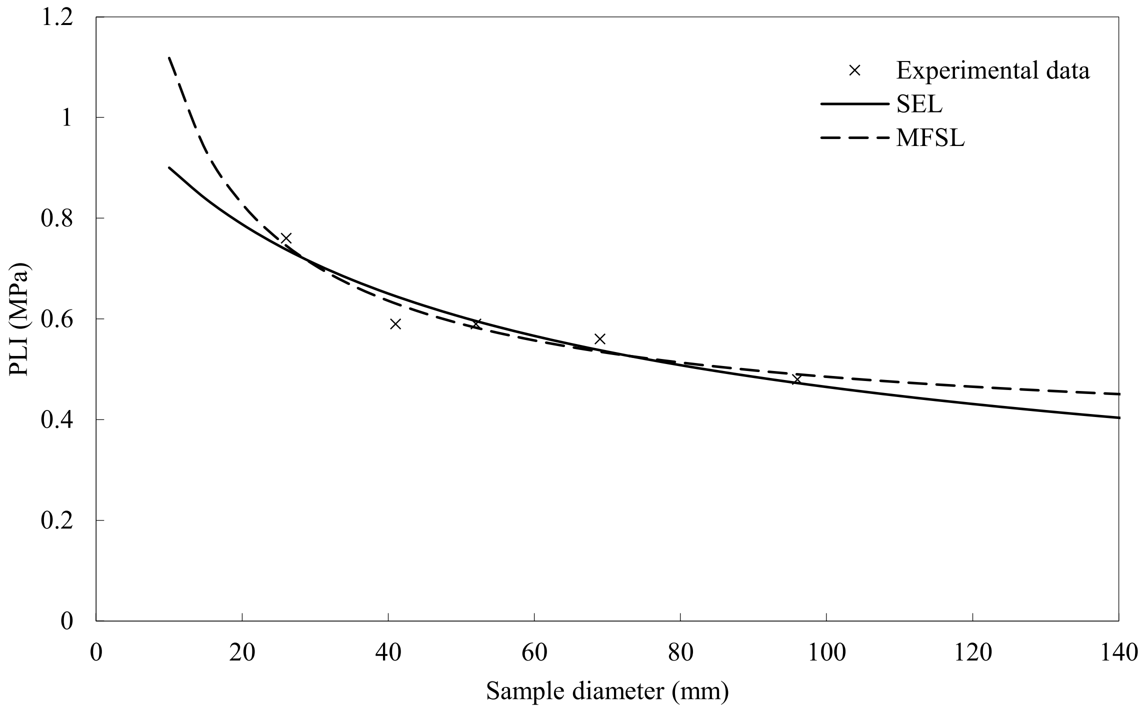

Fig. 26 Comparing SEL and MFSL predictions for axial PLI data obtained from Gambier limestone

Table 14 Correlation factors between UCS and PLI data for both axial and diametral conditions obtained from Gambier limestone

Sample diameter (mm)	Mean UCS (MPa)	Mean PLI (MPa)			
		Axial	*K*	Diametral	*K*
26	2.58	0.76	3.39	0.88	2.93
41	3.02	0.59	5.12	0.62	4.87
52	3.10	0.59	5.25	0.54	5.74
69	3.49	0.56	6.23	0.43	8.12
96	3.72	0.48	7.75	0.41	9.07

limestone and from 26 to 139 mm diameter for artificial rock. A set of uniaxial compressive, Brazilian and point load (axial and diametral) tests were conducted on Gambier limestone while only uniaxial compressive experiments were performed on artificial rock. Ascending then descending size effect trends were observed for both UCS data and Young's moduli obtained from Gambier limestone and artificial rock samples. The characteristic size for Gambier limestone was 119 mm diameter where the strength reduces before and beyond this size. The characteristic size for artificial rock was 52 mm diameter. The resulting size effect trend for Poisson's ratio was inconclusive similar to the earlier studies. The tensile strength and point load index (PLI) data obtained from Gambier limestone revealed only descending size effect trend as opposed to ascending and then descending size effect trend observed from UCS and elastic moduli data. Such a difference was attributed to the failure mechanism and contact points between the sample and the loading platens under Brazilian and point load testing which are different to those under uniaxial compressive loading.

The unified size effect law (USEL) and its improved version (IUSEL) were used for the strength prediction of large diameter samples. Initially, both USEL and IUSEL were calibrated using the laboratory data leading to a very good agreement between the model predictions and the experimental results. The analysis was performed on UCS data and Young's moduli obtained from Gambier limestone and artificial rock as well as the UCS data obtained from Bath stone reported in the literature. Hence, it was demonstrated that the strength prediction by IUSEL for a sample with an infinite scale is more realistic than that predicted by USEL. Also, the size effect law (SEL) and multifractal scaling law (MFSL) were fitted to the resulting tensile strength and PLI data obtained from Gambier limestone and showed that

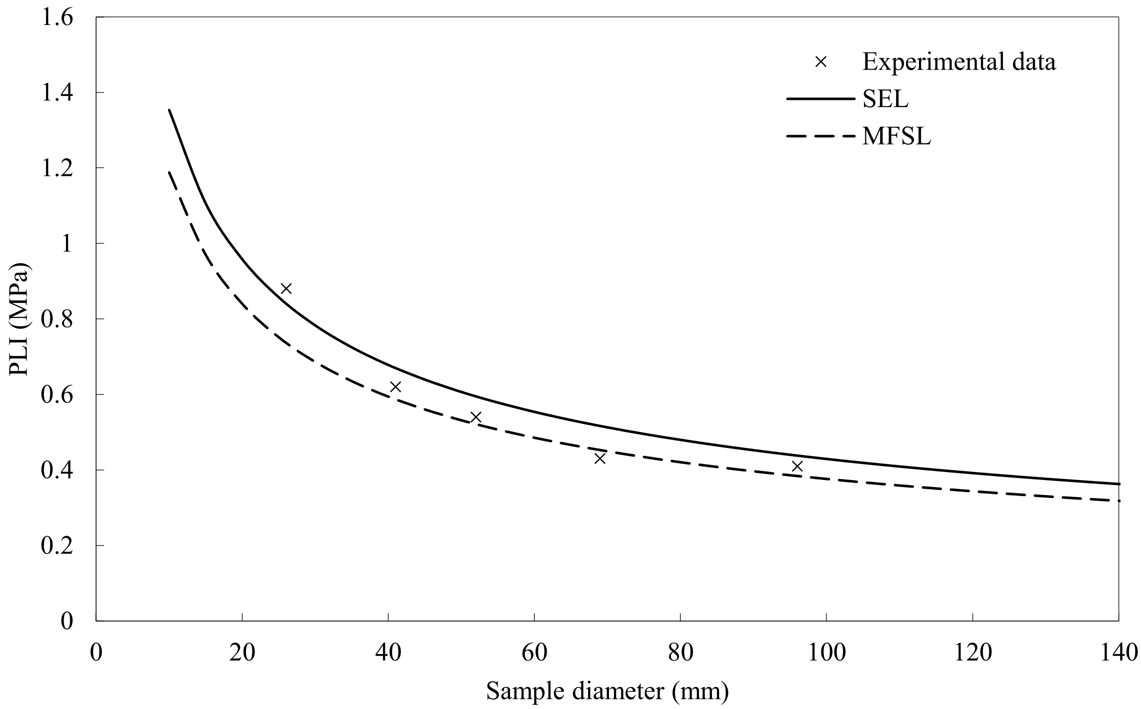

Fig. 27 Comparing SEL and MFSL predictions for diametral PLI data obtained from Gambier limestone

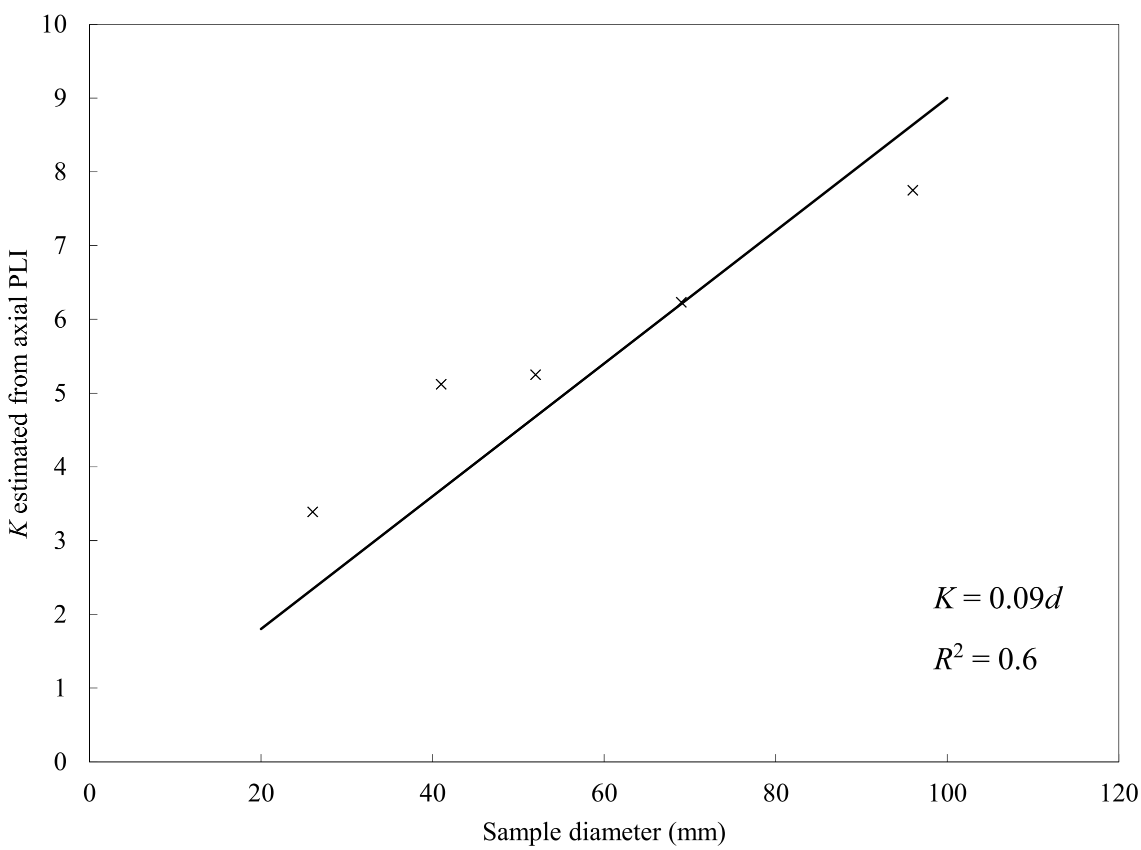

Fig. 28 Size correlation graph resulted from UCS and axial PLI of Gambier limestone

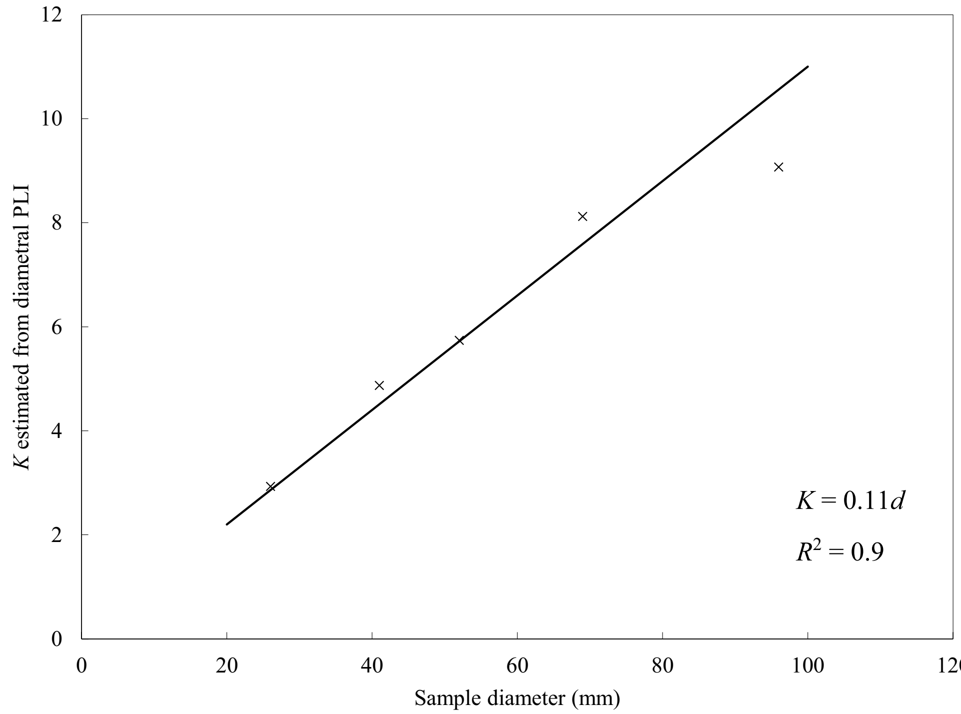

Fig. 29 Size correlation graph resulted from UCS and diametral PLI of Gambier limestone

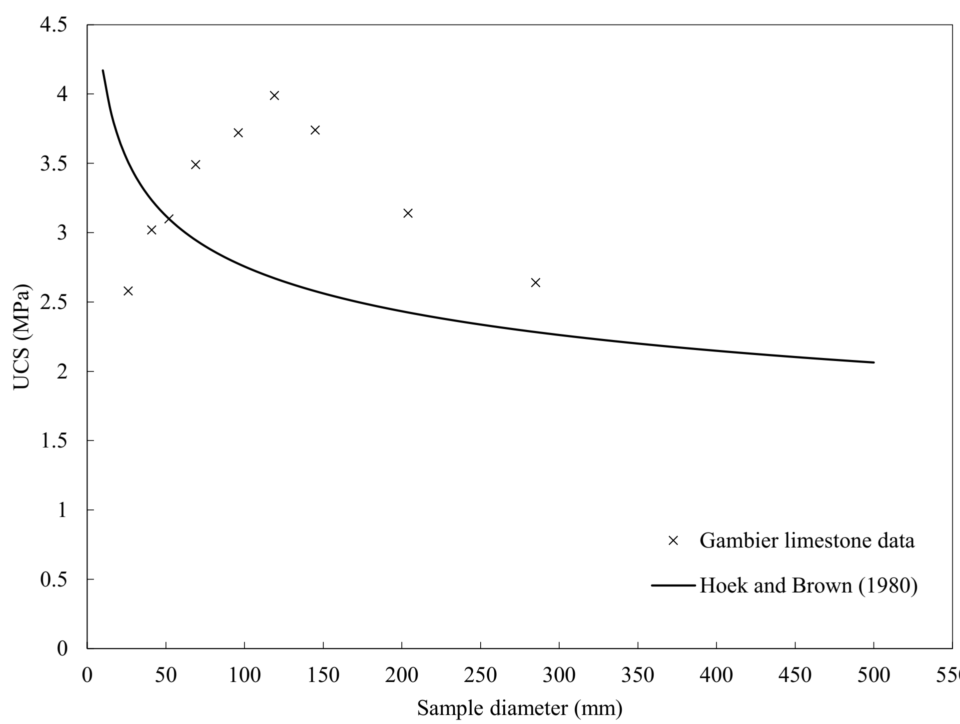

Fig. 30 Comparison between Hoek and Brown (1980) size effect model prediction and the experimental data obtained from Gambier limestone

MFSL is a good predictive model for PLI data while SEL found to be a better model for tensile strength data. Finally, an example of field application regarding the size correction in weak intact rocks was presented along with a methodology on how to estimate UCS from PLI at various sizes for weak intact rocks.

Acknowledgements The authors thank Australian Government Research Training Program (RTP) and Australian Coal Association Research Program (ACARP) funded project C25025 for their great support and contribution during the completion of this paper.

References

Allison G, Hughes M (1978) The use of environmental chloride and tritium to estimate total recharge to an unconfined aquifer. Soil Res 16:181–195

ASTM (2010) D7012-10 (2010) Standard test method for compressive strength and elastic moduli of intact rock core specimens under varying states of stress and temperatures. Annual Book of ASTM Standards. American Society for Testing and Materials, West Conshohocken

Bahrani N, Kaiser PK (2016) Numerical investigation of the influence of specimen size on the unconfined strength of defected rocks. Comput Geotech 77:56–67

Bazant Z (1984) Size effect in blunt fracture: concrete, rock, metal. J Eng Mech 110:518–535

Bazant Z (1997) Scaling of quasibrittle fracture: hypotheses of invasive and lacunar fractality, their critique and Weibull connection. Int J Fract 83:41–65

Bieniawski ZT (1968) The effect of specimen size on compressive strength of coal. Int J Rock Mech Min Sci 5:325–335

Carpinteri A, Chiaia B, Ferro G (1995) Size effects on nominal tensile strength of concrete structures: multifractality of material ligaments and dimensional transition from order to disorder. Mater Struct 28:311

Carpinteri A, Ferro G, Monetto I (1999) Scale effects in uniaxially compressed concrete specimens. Mag Concret Res 51:217–225

Clifton J (1973) Some aspects of the setting and hardening of gypsum plaster, vol 755. US National Bureau of Standards, New York

Cunha AP (1990) Scale effects in rock mechanics. In: The first international workshop on scale effects in rock masses. Loen, Norway, June 7–8 1990, pp 3–27

Darbor M, Faramarzi L, Sharifzadeh M (2018) Size-dependent compressive strength properties of hard rocks and rock-like cementitious brittle materials. Geosyst Eng 20:1–14

Darlington WJ, Ranjith PG, Choi SK (2011) The effect of specimen size on strength and other properties in laboratory testing of rock and rock-like cementitious brittle materials. Rock Mech Rock Eng 44:513

Dhir R, Sangha C (1973) Relationships between size, deformation and strength for cylindrical specimens loaded in uniaxial compression. Int J Rock Mech Min Sci Geomech Abstr 10:699–712

Dorbani S, Kharchi F, Salem F, Arroudj K, Chioukh N (2011) Influence of the addition of sand and compaction on the mechanical and thermal performances of plaster. Engineering 3:895

Faramarzi L, Rezaee H (2018) Testing the effects of sample and grain sizes on mechanical properties of concrete. J Mater Civ Eng 30:04018065

Hawkins AB (1998) Aspects of rock strength. Bull Eng Geol Environ 57:17–30

Hoek E (2000) Practical rock engineering

Hoek E, Brown ET (1980) Underground excavations in rock. Institution of Mining and Metallurgy, London

Hoskins JR, Horino FG (1969) Influence of spherical head size and specimen diameters on the uniaxial compressive strength of rocks, vol 7234. U.S. Dept. of the Interior, Bureau of Mines, Washington DC

ISRM (1978) International society for rock mechanics commission on standardization of laboratory and field tests. Suggested methods for the quantitative description of discontinuities in rock masses. Int J Rock Mech Min Sci 15:319–368

ISRM (1981) Rock characterization, testing and monitoring: ISRM suggested methods. ISRM, Oxford

ISRM (2014) The ISRM suggested methods for rock characterization, testing and monitoring: 2007–2014. Springer, Berlin

Jackson R, Lau J (1990) The effect of specimen size on the laboratory mechanical properties of the Lac Du Bonnet grey granite. In: The first interinaltional workshop on scale effects in rock masses. Loen, Norway, June 7–8 1990, pp 165–174

Li K, Cheng Y, Fan X (2018) Roles of model size and particle size distribution on macro-mechanical properties of Lac du Bonnet granite using flat-joint model. Comput Geotech 103:43–60

Masoumi H (2013) Investigation into the mechanical behaviour of intact rock at different sizes. Published, University of New South Wales

Masoumi H, Bahaaddini M, Kim G, Hagan P (2014) Experimental investigation into the mechanical behavior of Gosford sandstone at different sizes. In: 48th U.S. rock mechanics/geomechanics symposium. Minneapolis, USA, 2014, vol 2, pp 1210–1215

Masoumi H, Saydam S, Hagan P (2015) A modification to radial strain calculation in rock testing. Geotech Test J 38:813–822

Masoumi H, Saydam S, Hagan PC (2016a) Incorporating scale effect into a multiaxial failure criterion for intact rock. Int J Rock Mech Min Sci 83:49–56

Masoumi H, Saydam S, Hagan PC (2016b) Unified size-effect law for intact rock. Int J Geomech 16:04015059

Masoumi H, Roshan H, Hagan P (2017a) Size-dependent Hoek–Brown failure criterion. Int J Geomech 17:04016048

Masoumi H, Roshan H, Hagan P, Sharifzadeh M (2017b) An improvement to unified size effect law for intact rock. Paper presented at the 51st U.S. rock mechanics/geomechanics symposium, San Francisco, USA, 25–28 June

Masoumi H, Roshan H, Hedayat A, Hagan PC (2018) Scale-size dependency of intact rock under point-load and indirect tensile Brazilian testing. Int J Geomech 18:04018006

Melean Y, Washburn KE, Callaghan P, Arns CH (2009) A numerical analysis of NMR pore–pore exchange measurements using micro X-ray computed tomography. Diffus Fundam 10:301–303

Murray-Wallace C, Belperio A, Bourman R, Cann J, Price D (1999) Facies architecture of a last interglacial barrier: a model for Quaternary barrier development from the Coorong to Mount Gambier Coastal Plain, southeastern Australia. Mar Geol 158:177–195

Nishimatsu Y, Yamaguchi U, Motosugi K, Morita M (1969) The size effect and experimental error of the strength of rocks. J Soc Mater Sci Jpn 18:1019–1025

Panek LA, Fannon TA (1992) Size and shape effects in point load tests of irregular rock fragments. Rock Mech Rock Eng 25:109–140

Pells P (2004) On the absence of size effects for substance strength of Hawkesbury Sandstone. Aust Geomech 39:79–83

Pierce M, Gaida M, DeGagne D (2009) Estimation of rock block strength. In: Third CANUS rock mechanics symposium. Toronto, Canada, 2009, vol 1, pp 1–14

Quiñones J, Arzúa J, Alejano LR, García-Bastante F, Mas Ivars D, Walton G (2017) Analysis of size effects on the geomechanical parameters of intact granite samples under unconfined conditions. Acta Geotechn 20:1–14

Ridge M (1958) Effect of temperature on the structure of set gypsum plaster. Nature 182:1224

Rong G, Peng J, Yao M, Jiang Q, Wong LNY (2018) Effects of specimen size and thermal-damage on physical and mechanical behavior of a fine-grained marble. Eng Geol 232:46–55

Roshan H, Masoumi H, Hagan P On size-dependent uniaxial compressive strength of sedimentary rocks in reservoir geomechanics. In: 50th U.S. Rock mechanics/geomechanics symposium. Houston, US, 2016, pp 2322–2327

Russell AR, Muir Wood D (2009) Point load tests and strength measurements for brittle spheres. Int J Rock Mech Min Sci 46:272–280
Song H, Jiang Y, Elsworth D, Zhao Y, Wang J, Liu B (2018) Scale effects and strength anisotropy in coal. Int J Coal Geol 195:37–46
Symons I (1970) The effect of size and shape of specimen upon the unconfined compressive strength of cement-stabilized materials. Magazine of Concrete Research 22:45–51
Thuro K, Plinninger R, Zah S, Schutz S (2001) Scale effects in rock strength properties. Part 1: unconfined compressive test and Brazilian test. In: EUROCK 2001: Rock mechanics-a challenge for society. Espoo, Finland, 2001, pp 169–174
Walton G (2018) Scale effects observed in compression testing of stanstead granite including post-peak strength and dilatancy. Geotech Geol Eng 36:1091–1111
Weibull W (1939) A statistical theory of the strength of materials. Generalstabens litografiska anstalts förlag
Yoshinaka R, Osada M, Park H, Sasaki T, Sasaki K (2008) Practical determination of mechanical design parameters of intact rock considering scale effect. Eng Geol 96:173–186
Yuki N, Aoto S, Yoshinaka R, Yoshihiro O, Terada M (1995) The scale and creep effect on the strength of welded tuff. In: Yoshinaka R, Kikuchi K (eds) International workshop on rock foundation